



HAL
open science

On the ability to study regional hydrometeorological changes using GPS and GRACE measurements

Artur Lenczuk, Luis Olivera-Guerra, Anna Klos, Janusz Bogusz

► To cite this version:

Artur Lenczuk, Luis Olivera-Guerra, Anna Klos, Janusz Bogusz. On the ability to study regional hydrometeorological changes using GPS and GRACE measurements. *Progress in Earth and Planetary Science*, 2024, 11 (1), pp.63. 10.1186/s40645-024-00665-4 . hal-04839626

HAL Id: hal-04839626

<https://hal.science/hal-04839626v1>

Submitted on 16 Dec 2024

HAL is a multi-disciplinary open access archive for the deposit and dissemination of scientific research documents, whether they are published or not. The documents may come from teaching and research institutions in France or abroad, or from public or private research centers.




L'archive ouverte pluridisciplinaire **HAL**, est destinée au dépôt et à la diffusion de documents scientifiques de niveau recherche, publiés ou non, émanant des établissements d'enseignement et de recherche français ou étrangers, des laboratoires publics ou privés.

RESEARCH ARTICLE

Open Access



On the ability to study regional hydrometeorological changes using GPS and GRACE measurements

Artur Lenczuk^{1*} , Luis Olivera-Guerra², Anna Klos¹  and Janusz Bogusz¹ 

Abstract

Recently, an ongoing rise in temperature for both land and ocean areas is recorded resulting from the Earth's warming climate. As a result, droughts we observe are getting more frequent, longer and more severe, exerting sustained impacts on humans, ecosystems leading to famine, poverty, mass migration, or agricultural and economic losses. The changes in climate are successfully monitored by analyzing Total Water Storage (TWS). For years, TWS has been successfully determined using geodetic techniques, such as gravity field variations observed by the Gravity Recovery and Climate Experiment (GRACE) missions or station position changes monitored by the Global Positioning System (GPS). As well, geodetic-derived data can be applied successfully to study of hydrometeorological events. To quantify droughts characteristics at different temporal and spatial scales, we recalculate the vertical displacements to Drought Severity Indices (DSI). We find that DSI based on GPS and GRACE are positively correlated at over 80% of stations around the world, highlighting both Americas and Europe as the most correlated areas. To validate results, we compare DSI based on GPS/GRACE with the Global Land Water Storage (GLWS) hydrological model, the traditional climate indices, and temperature anomalies. We show that GPS-DSIs are strongly temporally consistent with both the Standardized Precipitation Index (SPI) and the Soil Moisture Index (SMI) climate indices at 85% of stations, indicating weakly correlated areas at mid-latitudes. We further show a high potential of geodetic data to assess drought characteristics within climate zones as well as global studies. We note that moderate conditions dominate for all climate zones, for which dry moderate conditions are observed for 40% of the months analyzed. As a result, we note warning conditions at least 52% of global stations with extreme drying DSI trends above a value of 2–3 per year. We note that the global water changes are dominated by 9 month droughts at over 72% of stations, indicating the average drought duration around 12, 14, and 15 months for GPS-, GRACE-, and GLWS-DSI, respectively. The obtained results from geodetic measurements more reliably characterize the type and phase of drought, as well as how these droughts cascade into freshwater, enabling appropriate mitigation strategies.

Keywords GPS, GRACE, Drought, Hydrometeorological events, Climate index, Köppen–Geiger climate zones

*Correspondence:

Artur Lenczuk
artur.lenczuk@wat.edu.pl

¹ Faculty of Civil Engineering and Geodesy, Military University of Technology, street gen. Sylwestra Kaliskiego 34, 00-908 Warsaw, Poland

² Laboratoire des Sciences du Climat et de l'Environnement, Institut Pierre-Simon Laplace (IPSL), CEA-CNRS, Université Paris-Saclay, Orme Des Merisiers, 91190 Gif-Sur-Yvette, France



© The Author(s) 2024. **Open Access** This article is licensed under a Creative Commons Attribution 4.0 International License, which permits use, sharing, adaptation, distribution and reproduction in any medium or format, as long as you give appropriate credit to the original author(s) and the source, provide a link to the Creative Commons licence, and indicate if changes were made. The images or other third party material in this article are included in the article's Creative Commons licence, unless indicated otherwise in a credit line to the material. If material is not included in the article's Creative Commons licence and your intended use is not permitted by statutory regulation or exceeds the permitted use, you will need to obtain permission directly from the copyright holder. To view a copy of this licence, visit <http://creativecommons.org/licenses/by/4.0/>.

1 Introduction

According to the National Oceanic and Atmospheric Administration (NOAA)'s Annual Climate Reports, the global surface temperature has increased by 1.1 °C above 1850–1900 in the last decade, with each consecutive year being the warmest on record for both land and ocean areas (<https://www.ncei.noaa.gov/>). The abrupt climate changes such as increases in temperature, atmospheric evaporative demand (Wehner et al. 2021), or other anthropogenic activities such as land use change, water demand, and management (van Loon et al. 2022) result in more frequent and severe droughts (Dai 2013) spanning months and even years (van Loon and Laaha 2015). The most negative impacts of drought include the redistribution of species diversity, agricultural and economic losses, the reorganization of ecosystems, water scarcity, famine, poverty leading to loss of life, mass migration, or redefining coverage of future climate zones (Zhang et al. 2020; Cui et al. 2021). For example, Qiu (2010) showed that the recorded precipitation decreases by 60% since 2009 has resulted in economic losses of 2.5 billion US dollars due to crop failure in China. Hence, revealing the problems in drought monitoring is one of the primary challenges to scientists in the twenty-first century (Rodell and Li 2023).

To monitor the impacts of climate changes scientifically, the single, composited, or modeled meteorological parameters or water storage components have been used (e.g., Scanlon et al. 2018; Rodell and Li 2023). Key variables such as temperature, snow water equivalent, and surface water or groundwater storage are measured point-wise (in situ) or are provided as climate and hydrological models. However, in situ measurements generally span a short period and observations are not commonly shared (Bhanja et al. 2019). In contrast, for climate and hydrological models, widely available parameters are provided almost in real time and include information from around the world. Nevertheless, their quality depends on a number of variables, such as the inaccuracy and shortcomings of input data, deficiencies (non-physical, empirical, or simplifications) in modeling assumptions, or the variety of forcing fields that impose simulation reliabilities. Consequently, model-derived parameters may either under- or overestimate real global (Scanlon et al. 2018; Schmied et al. 2021) or regional (Scanlon et al. 2016) hydrometeorological changes. For many years, modeled meteorological parameters or water storage components have been successfully used to quantify drought characteristics at different temporal and spatial scales. Several drought indices have already been defined, such as the Standardized Precipitation Evapotranspiration Index (SPEI; Vicente-Serrano et al. 2010), the Palmer Drought Severity Index (PDSI; Palmer 1965), or the Surface Water Supply Index (SWSI; Shafer and Dezman 1982). However,

they typically focus on only one hydroclimatic parameter, limiting reliable monitoring of the length and severity of droughts, and consequently are unable to represent the current climate scenario (Jain et al. 2015).

An alternative way to monitor climate change is to use the remote sensing-derived data provided by geodetic techniques, such as the Gravity Recovery and Climate Experiment (GRACE; Tapley et al. 2004) and the Global Navigation Satellite System (GNSS). The time-variable gravity sensed by GRACE has been successfully used to analyze global and regional mass variations in the hydrosphere, cryosphere, and oceans (Tapley et al. 2019) and is strongly correlated with both climate and anthropogenic variability (Scanlon et al. 2015). Among all, Pfeffer et al. (2021) emphasized that the Total Water Storage (TWS) changes from GRACE are spatially and temporally coherent with interannual signals driven by teleconnection modes such as NAO (North Atlantic Oscillation), ENSO (El Niño Southern Oscillation), PDO (Pacific Decadal Oscillation) or with short-term changes affected by extreme hydroclimatic events including droughts and floods (Scanlon et al. 2018; Klos et al. 2023). Besides, Niu and Yang (2006) and Sun et al. (2012) showed that GRACE annual and long-term signals can be used to calibrate and validate the global land surface as well as climate models. The site position series recorded by GNSS have been also extensively used to study hydrological variability (Knappe et al. 2019; Wang et al. 2022) through Earth's surface deformation mass load variations via the elastic load theory (Farrell 1972) or through inverse procedure to determine TWS changes (Argus et al. 2014). GNSS-observed displacements have been successfully used for studying changes in, e.g., water storage components (Knowles et al. 2020) as snow water equivalent (Ouellette et al. 2013), ice mass loss (Wang et al. 2017), or groundwater (Lenczuk et al. 2023). Generally, GNSS displacements are fairly consistent with GRACE-derived TWS with a correlation over 0.6 for most cases (e.g., Ferreira et al. 2019; Knowles et al. 2020). Furthermore, GNSS displacements indicate a strong dependence with monsoon climate signals (Materna et al. 2020), atmospheric or precipitation cycles (Han 2017) or hydrological model (Knappe et al. 2019). Argus et al. (2014) proved that GNSS-derived TWS changes show a high spatial and temporal coherency with regional water changes estimated from GRACE and hydrological models revealing the physiographic properties of the region and climate processes (Fu et al. 2015) indicating various meteorological phenomena (Milliner et al. 2018). As a consequence, a number of GNSS- and GRACE-based drought severity indices (DSI) have been used to improve the ability of drought monitoring at regional (e.g., Yao et al. 2022; Klos

et al. 2023) and global scales (e.g., Zhao et al. 2017; Gerdener et al. 2020) in the recent years.

In our research, we study global relationships of drought index based on geodetic measurements with hydrological, meteorological, and climatic changes. We estimate DSI series using vertical displacement time series observed by Global Positioning System (GPS) and derived from GRACE at 999 global GNSS stations. The reliability of the drought indices is overall assessed by comparisons to, e.g., traditional climate indices, meteorological variables, or literature. Here, we compare both GPS- and GRACE-derived DSIs (hereafter called “GPS-DSI” and “GRACE-DSI”) with DSI based on Global Land Water Storage (GLWS) hydrological model, two traditional climate indices (the Standardized Precipitation Index (SPI) and the Soil Moisture Index (SMI)), as well as global temperature anomalies and extreme events reported in the literature.

This paper makes a fivefold contribution to Earth and climate science. To the best of our knowledge, (i) there is still no global assessment of the impact of choosing different types of GRACE data on identifying droughts. We show that DSIs for both GRACE spherical harmonics and mascons are commonly spatially coherent; over 80% of analyzed stations are positively correlated with GPS-DSI. The highest agreement is observed in the mid-latitudes characterized by intense hydrometeorological extreme events. (ii) Secondly, we prove the high potential of geodetic data to study characteristics (intensity, category, duration) of droughts that are not registered by traditional climate indices. We find that moderate conditions and 9 month droughts dominate for time series from geodetic measurements. (iii) We are the first to identifying the roles of climate zones with droughts and floods globally by relating the characteristics of drought index variability, etc. We show strong temporal coherence of DSI series within the single climate group for all analyzed datasets. (iv) We are as well the first to set hot spot regions of wetting and drying conditions worldwide using DSI cumulated trend. We note drying tendencies at least 52% of stations for geodetic measurements, mainly low-latitude areas. (v) We study the regional correlations via cross-phase angle and period for Brazil, (for the first time) for Europe, Australia, and Africa regions. The obtained results indicate good agreement in amplitude and phase between GPS-DSI, GRACE-DSI, and SMI, for which both long- and short-term scales refer to dry and wet events recorded in the analyzed regions.

The article is organized as follows: in Sect. 2, we detail the used data such as satellite geodetic data, hydrological model, meteorological parameters, and assumed methodology. Section 3 includes an overview of the obtained

results with a detailed discussion. Then, the article is completed with conclusions.

2 Datasets and methods

2.1 GPS observations

We use the vertical displacements of GPS permanent stations distributed globally, except the Greenland and Antarctica areas. The 999 daily time series are provided by the Nevada Geodetic Laboratory (NGL; Blewitt et al. 2018) and are processed using the Precise Point Positioning (PPP) method in GipsyX software version 1.0 (see more details at: <http://geodesy.unr.edu/gps/ngl.acn.txt>). We eliminate the offsets (i.e., displacements due to crustal movements as earthquakes or technical, environmental, and human factors) using initially the NGL database and then manual inspection. The outliers are eliminated by applying the Inter-Quartile Range rule (IQR; Upton and Cook 1996). To correct the nontidal oceanic and atmospheric loadings, we use products provided by the Earth System Modelling Group of Deutsches GeoForschungsZentrum Section 1.3 (ESM GFZ; Dill and Dobsław 2013). To eliminate the postglacial rebound effect, we apply the ICE-6G_C model developed by Stuhne and Peltier (2015). Afterward, the daily GPS-observed displacements are averaged to monthly samples and truncated to January 2002 to December 2019 period to be consisted with GRACE and hydrological model.

2.2 GRACE and GRACE-FO monthly solutions

We use the spherical harmonic coefficients GRACE release 06 (RL06) and GRACE-FO RL06.1 provided by the Jet Propulsion Laboratory (JPL) at the California Institute of Technology (Yuan 2018, 2019) and the Center for Space Research (CSR) at the University of Austin (Betadpur 2018; Save 2019). Spherical harmonics represent gravity field variations up to degree and order 96 and are defined as the anomalies relative to GGM05C static gravity field model (Ries et al. 2016); note that nine months (four in 2004, three in 2012 and two in 2015) are available only up to degree and order 60 for JPL. The low-degree coefficients are replaced using Technical Note 14 (TN14) by following Sun et al. (2016) for degree-1, and the Satellite Laser Ranging (SLR) estimations for degree-2 and degree-3 coefficients. The details concerning all corrections are available at <https://podaactools.jpl.nasa.gov/>. To spatially average the spherical harmonic coefficients, we use two different filters, i.e., de-correlation DDK3 filter (“DDK”) and Gaussian smoothing with radius of 300 km (“Gauss”). Furthermore, we use recent solutions of mascons (RL06.1_v03 and RL06.2). Both JPL (Watkins et al. 2015) and CSR (Save et al. 2016) mascon solutions (hereafter abbreviated as “MSC JPL” and “MSC CSR”) have a global coverage and are provided on a 0.5° (MSC JPL) and

0.25° (MSC CSR) grid, simplifying the separation of signals between the ocean and land. The specific data processing details and used background models are available through <https://grace.jpl.nasa.gov/> and <https://www2.csr.utexas.edu/> websites. It should be noticed that for both GRACE data the missing months and the 11 months gap between both missions were filled using the autoregressive TWS reconstruction approach proposed by Lenczuk et al. (2022). To estimate GRACE-derived vertical displacements for GPS locations, TWS-gridded changes are converted into spherical harmonic coefficients (Wahr et al. 1998; Wang et al. 2017) up to degree and order (d/o) equal to 120 (Save et al. 2016) using Farrell load Love numbers (1972).

2.3 Drought Severity Index (DSI)

2.3.1 DSI estimation

To capture and assess the magnitude of the hydrometeorological events using satellite geodetic data, we calculate GPS- and GRACE-based DSI values using Zhao et al. (2017) approach, for which DSIs are defined as the standardized anomalies of vertical displacements (VD) caused by TWS changes as follows:

$$DSI_{i,j} = \frac{VD_{i,j} - \overline{VD}_j}{\sigma_j}, \quad (1)$$

where i and j mean year ranged from 2002 to 2019 and month from January to December, respectively. \overline{VD}_j and σ_j are the mean and standard deviation values of vertical displacements in month j . It should be noticed that displacements are assuming the Earth's elastic response to mass loading and reflect the opposite changes to TWS. Consequently, for wet conditions DSI is negative, while for dry conditions—positive. Thus, DSI detects both drought and wet events indicating exceptionally wet conditions for values less than -2.0 , extremely wet from -1.99 to -1.60 , very wet from -1.59 to -1.30 , moderately wet from -1.29 to -0.80 , abnormally wet from -0.79 to -0.50 , near normal conditions from -0.49 to 0.49 , abnormally dry from 0.50 to 0.79 , moderate drought from 0.80 to 1.29 , severe drought from 1.30 to 1.59 , extreme drought from 1.60 to 1.99 , and exceptional drought for values higher than 2.0 .

2.3.2 Reliability of DSIs

To assess the reliability of GPS-/GRACE-DSI and to get clearer insights of hydrometeorological events, we compare geodetic-based DSIs with (i) DSI determined from Global Land Water Storage (GLWS), (ii) climate indices such as the Soil Moisture Index (SMI) and the Standardized Precipitation Index (SPI), and (iii) the global surface temperature change (Table 1).

We use the newest 2.0 version of GLWS hydrological model with a spatial resolution of 0.5° per 0.5° within January 2003 to December 2019 period. Monthly GLWS TWS is derived by assimilating GRACE TWS changes into the Water-Global Assessment and Prognosis (WaterGAP) Global Hydrological Model (WGHM) via the Ensemble Kalman filter (Gerdener et al. 2023). GLWS includes the global anomalies of TWS excluding Greenland and Antarctica relative to January 2003 to December 2016 mean baseline. The missing months of GRACE data reflect the average of an assembly in which each element is dynamically consistent with the model. To be consistent with GPS and GRACE, GLWS TWS is recalculated to vertical displacements using converted spherical harmonic up to d/o equal to 360 (Wahr et al. 1998; Wang et al. 2017), and then, DSI is estimated following Zhao et al. (2017).

SMI is computed as weighted average of three parameters, i.e., root zone soil moisture from LISFLOOD model (<https://ec-jrc.github.io/lisflood-model/>), land surface temperature derived from Moderate Resolution Imaging Spectroradiometer (MODIS), and skin soil moisture defined by the Climate Change Initiative (CCI) European Space Agency (ESA) group (<https://climate.esa.int/en/>). The weights are calculated following Cammalleri et al. (2017) approach, and then, parameters are standardized on 2001–2016 period. SMI is calculated on a 30 days moving window and spans from January 2001 to December 2022. The product is globally provided at a 0.1° per 0.1° spatial resolution. We also use the SPI index as proposed by McKee et al. (1993). SPI is calculated using the historical precipitation anomalies from the Global Precipitation Climatology Centre (GPCC; <http://gpcc.dwd.de/>). Monthly SPI values are provided on a global grid of 1° per 1° for range of various timescales from 1 to 48 months since January 1981. Specifically, we use the SPI-12 product which reflects 12 months of accumulation period that is used to analyze hydrological changes (Secci et al. 2021).

In the case of global surface temperature change, we use the GISS Surface Temperature Analysis (Hansen and Lebedeff 1987) version 4 (GISTEMP v4) (Lenssen et al. 2019) that contains combined changes of sea surface temperature records and meteorological station measurements over land and ocean areas. GISTEMP represents values in an equal-area grid of 8000 boxes covering the Earth that are interpolated using the modified Kriging method. The data uncertainty is obtained using the fifth-generation European Centre for Medium-range Weather Forecasting atmospheric reanalysis (ERA5) and ERSSTv4 product provided by NOAA/NCEI (Huang et al. 2017).

Finally, SMI, SPI, and temperature values are interpolated to GPS locations using four surroundings values.

2.4 Study of consistency between DSIs

We quantify the consistency between GPS- and GRACE-based DSIs by means of two key metrics: the concordance correlation coefficient and the variance reduction. These metrics allow us to assess the similarity and agreement between the temporal patterns of GPS- and GRACE-derived datasets, considering both the correlation and amplitude aspects. Temporal coherence of GPS- and GRACE-DSI is assessed by estimating the concordance correlation coefficient (r_{xy} ; Lin 1989). Unlike Pearson's correlation coefficient, which only measures the strength of the linear relationship between two series, r_{xy} also considers the similarity in the amplitudes of two compared series. It is estimated using the following formula:

$$r_{xy} = \frac{\frac{2}{N} \sum_{k=1}^N (x_k - \bar{x})(y_k - \bar{y})}{\frac{1}{N} \sum_{k=1}^N (x_k - \bar{x})^2 + \frac{1}{N} \sum_{k=1}^N (y_k - \bar{y})^2 + (\bar{x} - \bar{y})^2}, \quad (2)$$

where x_k, y_k are two time series being compared for k -th time, \bar{x}, \bar{y} represent the means of x , and y . N is a number of observations (months) for both x and y time series.

To assess the consistency of amplitude and phase between GPS- and GRACE-DSI, we calculate variance reduction parameter following Gaspar and Wunsch (1989) approach:

$$\text{var}_{\text{red}} = \left(1 - \frac{\text{var}([GPS - \text{DSI}] - [GRACE - \text{DSI}])}{\text{var}([GPS - \text{DSI}])} \right) \cdot 100. \quad (3)$$

It is assumed that var_{red} values greater than 50% represent agreement between GPS- and GRACE-DSI in phase and amplitude (Peidou et al. 2023). Values of 100% mean perfect consistency. Negative values appear with large differences in amplitude and phase.

We further utilize the wavelet coherence parameter to analyze the relationship between GPS-DSI and other datasets, including GRACE, GLWS, and SMI. It allows to determine the correlation between two selected datasets in the time–frequency space. The wavelet coherence is based on the analytic Morlet wavelet (Kronland-Martinet et al. 1987) and is computed using (Azad et al. 2022):

$$\frac{|S(C_x^*(a, b)C_y(a, b))|^2}{S(|C_x(a, b)|^2) \cdot S(|C_y(a, b)|^2)}, \quad (4)$$

where $C_x(a, b)$ and $C_y(a, b)$ denote the continuous wavelet transforms of x and y time series at scales a and time b of the wavelet transform. $C_x^*(a, b)$ is the complex conjugate of $C_x(a, b)$, and S indicates the smoothing over both time and scale.

3 Results and discussion

3.1 Consistency between GPS- and GRACE-based DSIs

3.1.1 Concordance correlation coefficient and variance reduction

In Fig. 1, we present the maps of concordance correlation coefficient (left column) and variance reduction (right column) values calculated between DSI based on GPS and different types of GRACE JPL data. In the case of r_{xy} , we find over 80% of stations being positively correlated with GPS for all GRACE data; at least 30% of stations are characterized with correlation greater than 0.5. In case of mascons, we obtain the largest r_{xy} for stations located in both Americas and Europe, mostly in the central parts of the continents, for which r_{xy} over 0.6 is predominant. For spherical harmonics coefficients, we get values comparable to mascons in spatial and temporal domain, although spherical harmonics yield smaller r_{xy} compared to mascons, with values being 0.1 and 0.2 lower for 20% and 30% of stations situated, respectively, in the central parts of North America and Europe. For both mascons and spherical harmonics, negatively correlated stations are found at single points spread around the world, mostly over island and coastal areas. We observe almost 5% more negatively correlated stations for spherical harmonics relative to mascons. We notice that the regions with maximum correlation overlap with extreme TWS trends (e.g., central USA or southern Brazil) and TWS annual amplitudes (e.g., Amazon river basin, eastern Africa, or southern Europe) areas described by Scanlon et al. (2018). Moreover, they spatially coincide with areas undergoing high precipitation anomalies, as documented by Gu and Adler (2023). Specifically, the precipitation anomalies are prevalent in subtropical and mid-latitude regions, including central parts of North America and South America, southwest USA, northern part of Australia, tropical west and southern parts of Africa, and Eurasia. Then, we analyze the results for stations located within the four main climate groups according to the Köppen–Geiger classification (Kottek et al. 2006), i.e., tropical (red), (semi-) arid (yellow), temperate (green), and continental (purple areas) (background colors in Fig. 1). The tropical climate covers near the equator areas, mainly within 15° N and S latitude. Through the low (mostly from 15 to 30°) latitude in both hemispheres, a (semi-)arid climate group is located. The temperate and continental zones cover the middle and high latitudes, mostly from 25° to 70° N and S. Since GLWS does not include TWS changes for Greenland and Antarctica ice sheets, we exclude latitudes higher than 60° in both hemispheres that represent polar climate zone. Within individual climate zones, we get the largest median concordance with GPS for continental and temperate zones equal to 0.4 and 0.3 for mascons and spherical harmonics, respectively. In (semi-)

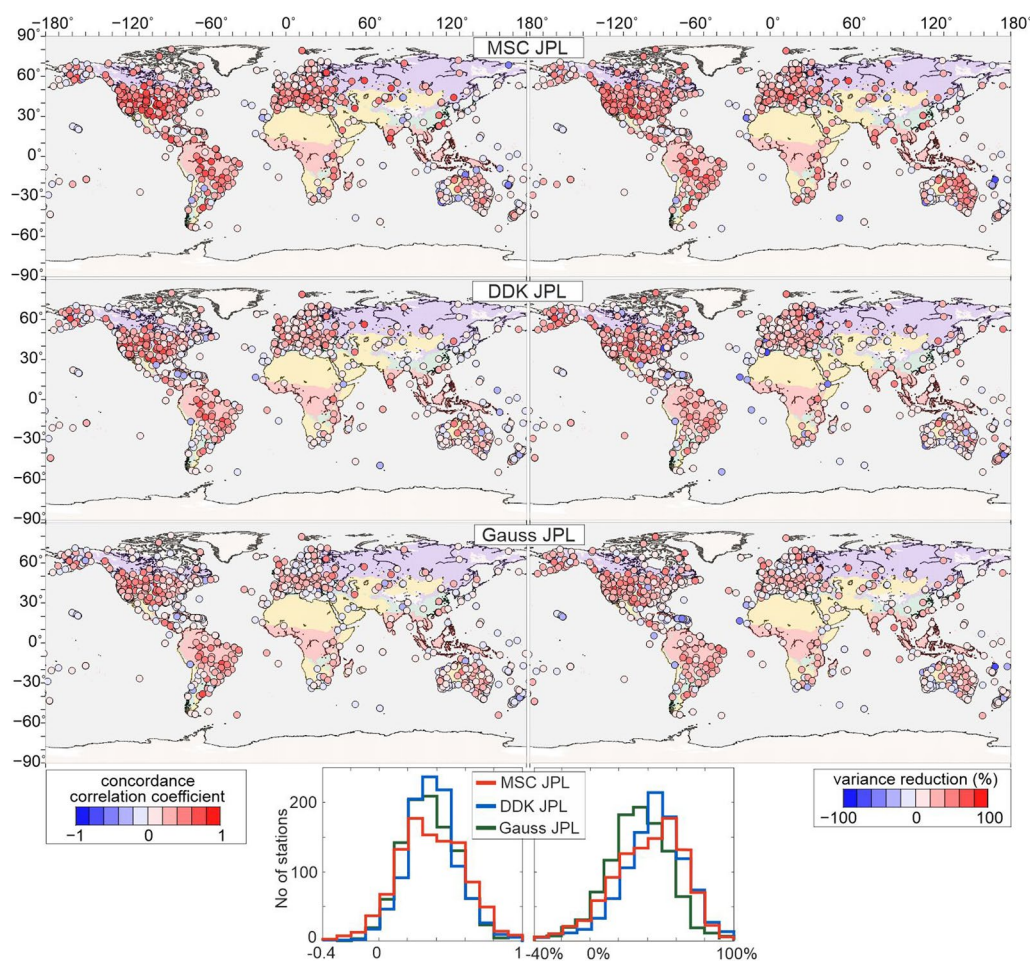


Fig. 1 Concordance correlation coefficient (left column) and the variance reduction (right column) estimated between GPS- and various GRACE-based DSI series determined from vertical displacements. Two different forms of GRACE data, i.e., mascon solution (“MSC JPL”; top map) and spherical harmonic coefficients (middle and bottom maps), are used. We use two various spatial averaging of spherical harmonic coefficients, i.e., DDK3 filter (“DDK JPL”; middle map) and Gaussian smoothing with radius of 300 km (“Gauss JPL”; bottom map). The histograms of concordance correlation coefficient (left column) and the variance reduction (right column) of DSIs estimated for selected 999 stations are presented for all used datasets. The background represents the four main climate groups according to the Köppen–Geiger climate classification scheme: tropical (red), (semi-)arid (yellow), temperate (green), and continental (purple)

arid and tropical zones, the median r_{xy} is smaller by 0.1. It is explained by a large number of negatively correlated stations located in Asia and Australia. In other regions within (semi-)arid and tropical climate zones, such as Amazon, south and east parts of Africa, the r_{xy} exceeds 0.4.

Then, following Peidou et al. (2023) we analyze the variance reduction (Fig. 1, right column) to assess the consistency of amplitude and phase between DSI determined from GPS and GRACE. The obtained results are spatially comparable to extreme values of concordance. Overall, the results highlight better consistency between GPS-DSI and mascon-derived GRACE-DSI compared to those obtained from spherical harmonics. We observe the

higher DSI agreement for central parts of both the Americas and Europe. For mascons, positive var_{red} is found at 91% of stations. The maximum values are dominant in inland areas with median values equal to 35%. The main disagreement with GPS is noticed along the coasts of continents and in Western Australia. In the case of spherical harmonics, we get positive var_{red} for 9% and 17% of stations less than for mascons using, respectively, DDK and Gaussian filters. The median values are around 24% for both filters. The poor agreement occurs at stations located on the east coast of the USA and South America, the western part of Australia, and the island areas. Regions exhibiting var_{red} values exceeding 50% in both GRACE datasets, including the central parts of North

America, Brazil, and southern parts of Europe, coincide with areas experiencing substantial long-term climate changes and human activities. These changes encompass variations in precipitation (increase or decrease), transitions between dry and wet periods, depletion of groundwater, and expansion of irrigation agriculture (Rodell et al. 2018). The highest agreement is also observed for regions of most intense hydrometeorological (drying/wetting) events occurring in the mid-latitudes, i.e., central and north parts of North America, Europe, South and East Africa, and central part of South America (Rodell and Li 2023). The observed local inconsistency may be explained by differences in GRACE root data processing (e.g., leakage effects, spatial filtering, mascon definition) or GPS error sources (such as multipath effects, ephemeris error, or error due to orbital eccentricity). Studying the results for the individual climate zone, the results are similar for both type of GRACE datasets (mascon and spherical harmonic) and both used spatial filters (“Gauss” and “DDK”) (Fig. 1). We notice agreement in amplitude and phase between GPS- and all three GRACE-based DSIs for over 70% of stations located at continental zone. For the other climate groups, at least 50% of stations for GRACE (i.e., both forms of data and both spatial filters) are in agreement with GPS, excluding only GRACE spherical harmonic smoothed by Gaussian filter within the tropical zone. We get the median values up to 30% for continental zone, and 20% for (semi-)arid and tropical zones for both GRACE mascons and spherical harmonics datasets (Table 2).

3.1.2 Correlation and RMS

We study the relationship of correlation between DSIs and RMS of DSI differences (Fig. 2) to assess the temporal consistency between GPS and GRACE. The dot colors present the results obtained for different climate zones i.e., tropical (A), (semi-)arid (B), temperate (C), and continental (D) that allow to analyze changes in different climate groups. Overall, we notice similar correlation across all pairs of datasets, for which increasing values correspond to decreasing RMS. Positively correlated stations dominate for all climate groups and all GRACE data. The slopes of linear relationships between correlation and RMS of differences values estimated from GPS and GRACE range from -0.9 to -0.7 for all climate zones. It reveals an almost (inversely) proportional relationship between RMS of DSI differences and correlation. The smallest slope value is found for tropical zone; however, slope is almost twofold for continental zone for all GRACE datasets. The large changes for continental zone are related with RMS of differences over 2.5 for correlations between -0.1 and 0.1 that we observe at stations located in the north part of North America and Scandinavia. For the other climate groups, we get the slope values equal to -0.7 and RMS around 1.3. The largest correlations and smallest RMS are mostly found at inland stations for which strong r_{xy} and var_{red} (Fig. 1) are noticed.

3.1.3 Comparison of DSI based on GRACE data provided by JPL and CSR processing centers

We then perform similar calculations to those shown in Figs. 1 and 2; however, we compare GRACE

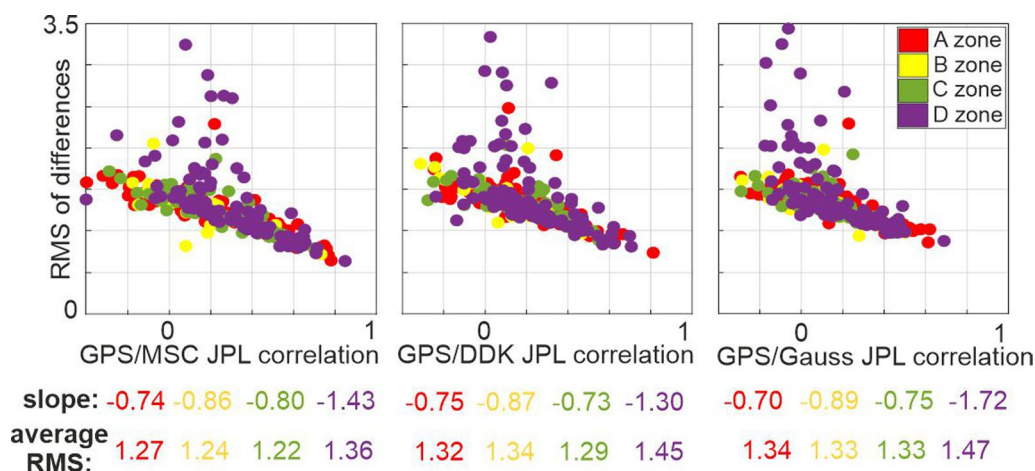


Fig. 2 RMS of difference calculated between GPS-DSI and GRACE-DSI with respect to correlation. We present results obtained for mascon solution (“MSC JPL”; left graph), and spherical harmonic coefficients filtered by DDK3 (“DDK JPL”; middle graph) and Gaussian smoothing with radius of 300 km (“Gauss JPL”; right graph) provided by JPL. The colored dots present the results obtained for four main climate groups according to the Köppen–Geiger classification, i.e., A—tropical (red), B—(semi-)arid (yellow), C—temperate (green), and D—continental (purple)

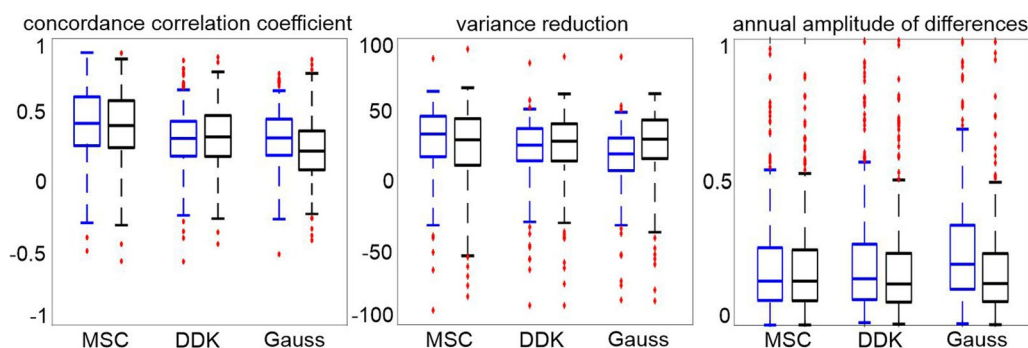


Fig. 3 Descriptive statistics of concordance correlation coefficient (left graph), variance reduction (middle graph) and annual amplitude of DSI differences (right graph) between GPS-DSI and GRACE-DSI. Blue and black boxes represent GRACE data provided by JPL and CSR processing centers, respectively. On each box, the central mark indicates the median, and the bottom and top edges of the box indicate the 25th and 75th percentiles, respectively. The whiskers extend to the most extreme data points not considered outliers; however, the outliers are plotted individually using the red dots

mascon solution and spherical harmonics provided by CSR processing center (Table 2 and Fig. 3). We compare the obtained GRACE-DSI from both CSR and JPL centers by determining the r_{xy} , var_{red} , and the annual amplitude of DSI differences estimated between GPS and GRACE. The results are presented in Fig. 3, indicating the median with the 25th and 75th percentiles values as the bottom and top edges of the box, and the individually outliers plotted using red dots. We note significant resemblance between JPL (blue) and CSR (black boxplots) datasets. The r_{xy} values are almost identical for both GRACE JPL and CSR datasets. However, the median values are about 0.1 greater for mascons than for both spherical harmonics. We observe the weakest correlations between GPS and GRACE spherical harmonics spatially averaged using Gaussian smoothing (Fig. 3, left graph). Very similar results are found for var_{red} parameter (Fig. 3, center graph). Median values are within 20–30% for all GRACE datasets. For JPL mascon solution, we note better GRACE agreement with GPS and less divergence of DSI values compared to CSR. For spherical harmonics, DSI values are about 5% and 10% greater, respectively, for DDK and Gaussian smoothing for both JPL and CSR. We show that seasonal variations between GPS- and

GRACE-DSI series are minor (Fig. 3, right graph). The median annual amplitude of DSI differences is up to 0.2, excluding GRACE JPL spatially averaged using Gaussian smoothing with median equals to 0.3. Almost 75% of the stations are characterized with an amplitude of difference of less than 0.5. Moreover, we notice amplitudes greater by 0.2 and 0.1, respectively, for JPL spherical harmonics filtered using DDK and Gaussian smoothing.

We further analyze the spatial coherence of results we obtained for GRACE datasets provided by JPL and CSR. The values of concordance with GPS are consistent at least 92% of stations for both GRACE centers. 90% of stations are positively correlated and at least 25% of them are correlated over 0.5. The differences occur mainly at unrelated stations scattered over the world. For example, for JPL we find concordance smaller by 0.3 than for CSR at 5% of stations for spherical harmonics. The largest discrepancies between data from both centers are observed for entire Australia (except eastern part of continent) for spherical harmonics, and its western and northern parts for mascon solutions (not shown). For example, we obtain concordance smaller by 0.2 for CSR than for JPL for both GRACE mascons and spherical harmonics in West Australia. In the case of amplitude, we find that

Table 1 Data used for calculations

	Data availability	Spatial resolution	Temporal resolution	Analyzed data	Source
GPS	1994–present	Point	Days	Monthly data for 01/2003–12/2019	NGL
GRACE	04/2002–present	~200–300 km	Months		CSR, JPL
GLWS	01/2003–12/2019	0.5°	Months		University of Bonn
SMI	01/2001–12/2022	0.1°	Months		Global Drought Observatory
SPI	01/1981–12/2021	1°	Months		Global Drought Observatory
Temperature	01/1880–12/2023	2°	Months		NASA Goddard Institute for Space Studies

Table 2 Statistics calculated for concordance correlation coefficient and variance reduction estimated between GPS- and GRACE-DSIs

GRACE data type	Parameter	Concordance correlation coefficient				Variance reduction (%)			
		A	B	C	D	A	B	C	D
MSC	Mean	0.41	0.39	0.44	0.48	23	22	28	38
JPL	Median	0.38	0.35	0.42	0.41	21	25	26	36
	Minimum	-0.42	-0.51	-0.44	-0.42	-46	-36	-40	-21
	Maximum	1.00	1.00	1.00	1.00	83	93	99	96
DDK	Mean	0.25	0.24	0.32	0.35	19	21	27	34
JPL	Median	0.27	0.22	0.32	0.33	21	25	29	35
	Minimum	-0.42	-0.56	-0.47	-0.26	-49	-42	-55	-24
	Maximum	1.00	1.00	1.00	1.00	96	89	98	93
Gauss JPL	Mean	0.23	0.25	0.33	0.36	22	23	24	32
	Median	0.21	0.25	0.31	0.33	20	22	25	34
	Minimum	-0.32	-0.51	-0.30	-0.24	-53	-44	-48	-25
	Maximum	1.00	1.00	1.00	1.00	90	88	98	93

The statistic are calculated for different climate zones i.e., tropical (A), (semi-)arid (B), temperate (C), and continental (D)

negatively correlated stations are characterized with 0.1 smaller amplitudes of DSI for CSR mascons. For spherical harmonics, the largest discrepancies are found at stations with correlation ranging from -0.1 to 0.1. It is noticed at stations located at different climate zones and probably stems from the application of different background models in both type of GRACE data.

3.2 GPS-DSI comparison to traditional climate indices

The climate changes are commonly analyzed using traditional climate indices based on modeled meteorological parameters. Hence, to assess the reliability of

GPS-DSI to study hydroclimatic and hydrometeorological changes we analyze anomaly correlation coefficients between GPS-DSI, and SPI and SMI that are based on precipitation and soil moisture (Fig. 4), respectively. The presented maps point to related spatial patterns of correlation for both traditional climate indices with GPS-DSI. We note a similar change at 85% of stations and correlation greater than 0.5 for 39% and 47% of them, respectively, for SPI and SMI. Nonetheless, there are some unambiguous regions such as Australia, Oceania, and the northwest part of Europe, which are characterized with correlations lower by 0.2–0.3 for SPI

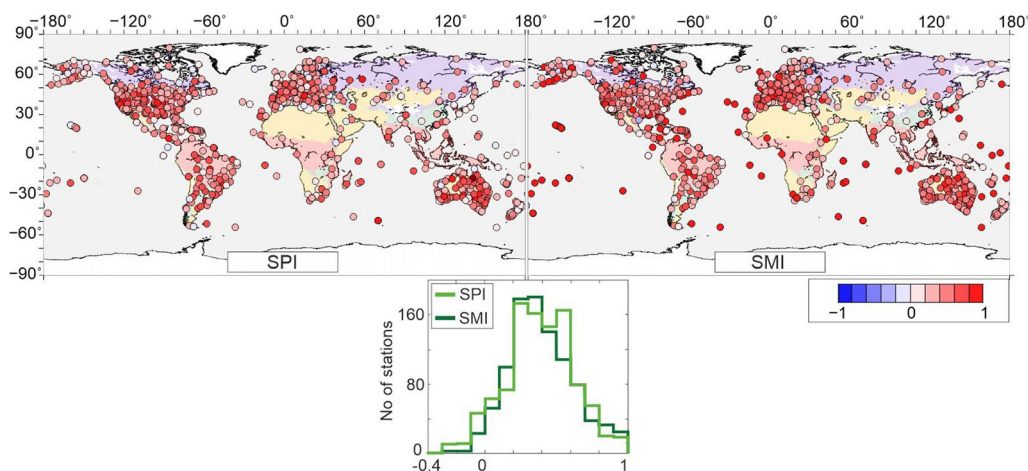


Fig. 4 Anomaly correlation coefficient estimated between GPS-DSI and two traditional climate indices: SPI and SMI. The histogram of anomaly correlation coefficient of DSIs estimated for selected 999 stations is presented for both climate indices. The background represents the four main climate groups according to the Köppen–Geiger climate classification scheme: tropical (red), (semi-)arid (yellow), temperate (green), and continental (purple)

compared to SMI. As a result, the average correlation values are greater by 0.1 for SMI than for SPI. Nevertheless, for both cases the strongest agreement are found for near the equator and low-latitude areas. The weakly correlated areas occur mostly on middle latitudes, which are affected by different variables. For example in Latin America, sensitivity to warming of ocean water may contribute to the observed differences (Sutton 2018). In the central part of Asia, Zhang et al. (2019) showed that the discrepancies may stem from under-/overestimation of the dominant TWS components such as groundwater and snow water equivalent. In the case of the individual climate groups, we notice two major similarities of GPS-DSI and climate indices. First, in the (semi-)arid zone, 50% of stations are characterized with anomaly correlation greater than 0.5 for both SPI and SMI indices. The observed good agreement at only half of the number of stations is probably a consequence of the limited impact of precipitation and potential evapotranspiration in extremely arid area (Cammalleri et al. 2017; Řehoř et al. 2023). Second, we obtain the lowest agreement for the continental zone, for which the anomaly correlation exceeding 0.5 shows a notable similarity between SMI and SPI, with SPI exhibiting this characteristic in only 6% more stations (i.e., 31% of stations). However, the median value of correlation for SPI remains higher by 0.1 compared to SMI. For other two analyzed climate zones, we get a stronger agreement

between GPS-DSI and SMI for which we note correlation higher by an average of 0.2 than for SPI. This agreement between GPS and SMI may be explained by the observed decrease in soil relative available water, as monitored by GPS. This decrease has been identified as significant ‘hotspots’ areas by Řehoř et al. (2023), with a water decrease by 5% per decade.

3.3 Drought characteristics: duration and severity

Then, we focus on assessment of the characteristics of droughts using geodetic techniques. We determine the (median) drought duration and its category using GPS and GRACE data, and we compare them with results obtained from GLWS model (Fig. 5). The drought duration is defined as the number of months between the start and end of the drought (Mao et al. 2017) and is estimated as sum of duration of all droughts divided by the total number of their occurrences (Xu et al. 2019). However, to exclude any non-real changes stemming from geodetic techniques we take for DSI analysis only the periods lasting at least 3 months. We obtain the median length of drought around 12, 14, and 15 months for GPS, GRACE and GLWS, respectively. Droughts longer than 1 year occur mostly in a nearly unbroken belt around the Earth at low latitudes, mostly within 15° in both hemispheres. The longest droughts (even up to 2 years and longer) are found at mid-latitudes areas (e.g., central and western parts of North America, eastern part of

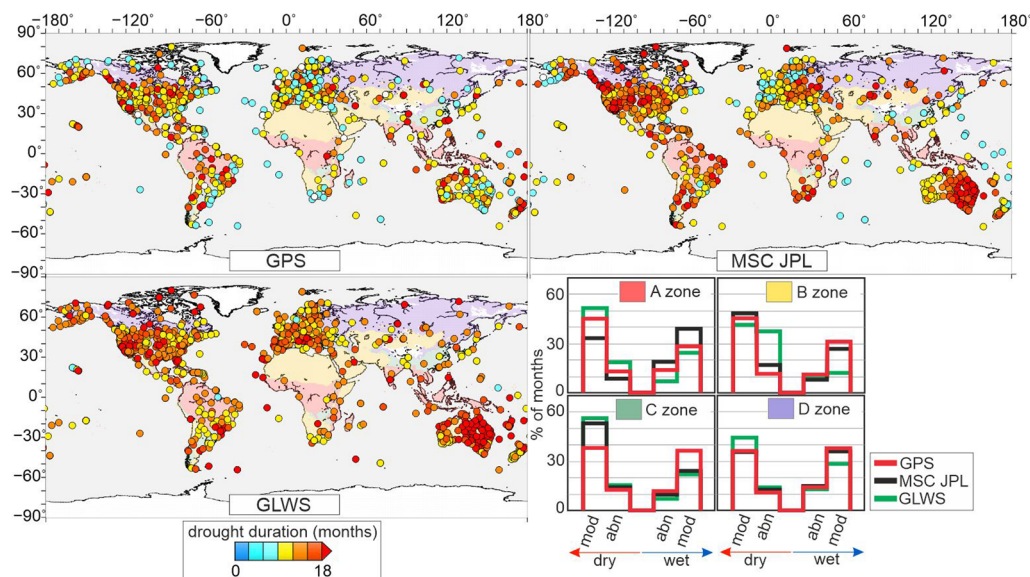


Fig. 5 Median drought duration estimated using GPS-, GRACE-, GLWS-DSI based on vertical displacements. GRACE-based determinations are obtained with the use of JPL mascon solution. The background represents the four main climate groups according to the Köppen–Geiger climate classification scheme: tropical (red), (semi-)arid (yellow), temperate (green), and continental (purple). The histograms present the proportion of the number of months (in %) of dominated drought category i.e., abnormal (“abn”) and moderate (“mod”) dry/wet conditions within analyzed 2002–2019 period. Results are presented for each climate zone for GPS-, GRACE- and GLWS-DSI (red, black and green curves, respectively). Note that the normal condition dominated for all climate zones is eliminated and is not presented in histograms

South America) for all datasets (Fig. A1). The results of the longest droughts are similar, but there are also some exceptions such as in Europe, to which we obtain shorter droughts for GPS. As a consequence, the number of droughts is greater for GPS than for GRACE and GLWS. For example, for GRACE and GLWS 1 year droughts are also obtained in drought-prone regions (Meza et al. 2020) such as Europe (except the western part of continent), eastern part of Africa, and Australia. It is also captured by GPS; however, there are observed hotspots covering smaller regions than sensed by GRACE and modeled using GLWS, marked by orange and red dots in Fig. 5 or red and black dots in Fig. A1 (left column). We also find much more droughts for GPS than for others data in Europe, north part of Asia, whereas more droughts are noticed for south part of Africa and west part of Australia for GRACE and GLWS (maps in right column). The smallest and largest number of droughts we obtain coincides, respectively, with the most intense areas of wet and dry periods presented by Rodell and Li (2023). The indicated regions in Europe, Africa, and Australia coincide with extreme drought duration trend estimated by Zeng et al. (2022) using climate indices and for which trend is greater than 1 month per decade. Moreover, these regions are under drought over 50% of the analyzed time that are simulated by different configurations of HadCM3C climate model and PDSI climate index (Taylor et al. 2012). We find that 9 month droughts predominate, occurring at 72%, 87%, and 95% of stations, respectively, for GPS, GRACE, and GLWS. GPS reveals droughts shorter than 9 months occur mostly on island or even in coastal areas. For GPS and GRACE, we also notice some 6 month droughts for eastern Europe that coincide with the 3–6 month periods of European rivers discharge (Eriyagama et al. 2009). In the case of the climate zones analysis, at least 9 months droughts are observed at more than 70%, 80%, and 90% stations, respectively, for GPS, GRACE, and GLWS. The median length of drought is about 12 months for tropical, temperate, and continental climate groups for all used datasets. For (semi-)arid zone, the median drought duration is 13 months for GPS, while for GRACE and GLWS is over 15 months. In the case of individual stations analysis, the longest droughts monitored by DSIs series span from 2 years for stations located at tropical zone (east part of South America) to as long as 4 years for stations located at continental zone (west and central parts of North America). Further, we study the frequency of occurrence of the dominant drought categories in single climate zones; however, we exclude the normal condition that is predominant in each zone. Results are presented as histograms in Fig. 5. The drought category for GPS, GRACE, and GLWS data is classified following the approach proposed by Zhao et al.

(2017). We note coherent results for used datasets for which moderate drought conditions (i.e., DSI from 0.80 to 1.29) dominate for all climate zones. They are found for at least 60% of the analyzed months. The dry conditions are observed for at least 40% of months of GRACE- and GLWS-DSI series for tropical, (semi-)arid, and continental zones. For GPS-DSI, we note the similar number of dry and wet months. Nevertheless, there are significant differences between all datasets, notably for stations located in (semi-)arid zone. We notice that mainly GLWS overestimates the drought category observed by GPS and GRACE and shows abnormal dry conditions (i.e., DSI from 0.5 to 0.79) for almost 40% of months.

3.4 Wetting and drying areas

We classify regions into hotspot regions of intensively drying and wetting regions and estimate the linear trend of cumulated DSI values (Fig. 6). Global drought conditions analysis of GPS-DSI indicates some hotspots of trends that overlap with significant DSI trends estimated using GRACE and GLWS. The drying tendencies are mainly identified in low-latitude regions such as Australia, South Africa, northern part of South America, and northeastern part of North America that are characterized with DSI trend greater than 2–3 per year (DSIs are unitless). The Australian, South African, and American regions coincide with the strongest and most robust droughts projected by CMIP5 and CMIP6 climate models (Ukkola et al. 2020). Overall, the wetting trends are noticed at 52% of stations for GPS-, and at 65% and 56% of them for GRACE- and GLWS-determined DSIs, respectively. We indicate that the number of dry events increased in the second half of the analyzed period, while the number of wet events is consistently decreasing. It could have direct consequences for food availability, people migration, or regional conflicts in the coming years. The almost areas with positive trends agree well with regions characterized by estimated temperature rate above 0.1 °C/yr (Fig. 6, bottom map) and drying trends determined by Jensen et al. (2019) from CMIP5 models. They have been already noted drying conditions for Europe, especially for western, central, and eastern areas, for which GPS-DSI indicates drying with hotspot regions of wetting. The most significant wetting conditions are found in the eastern parts of North America, Asia, and a few stations in the south parts of South America for GPS, GRACE, and GLWS. Nonetheless, there are some regions indicating different conditions. For example, GLWS-DSI reports wetting trends compared to GRACE-DSI drying trends for the west part of North America. It is probably related to underestimation of TWS changes by model for registered dry to wet progression period (Rodell et al. 2018). The significant climate changes are also registered

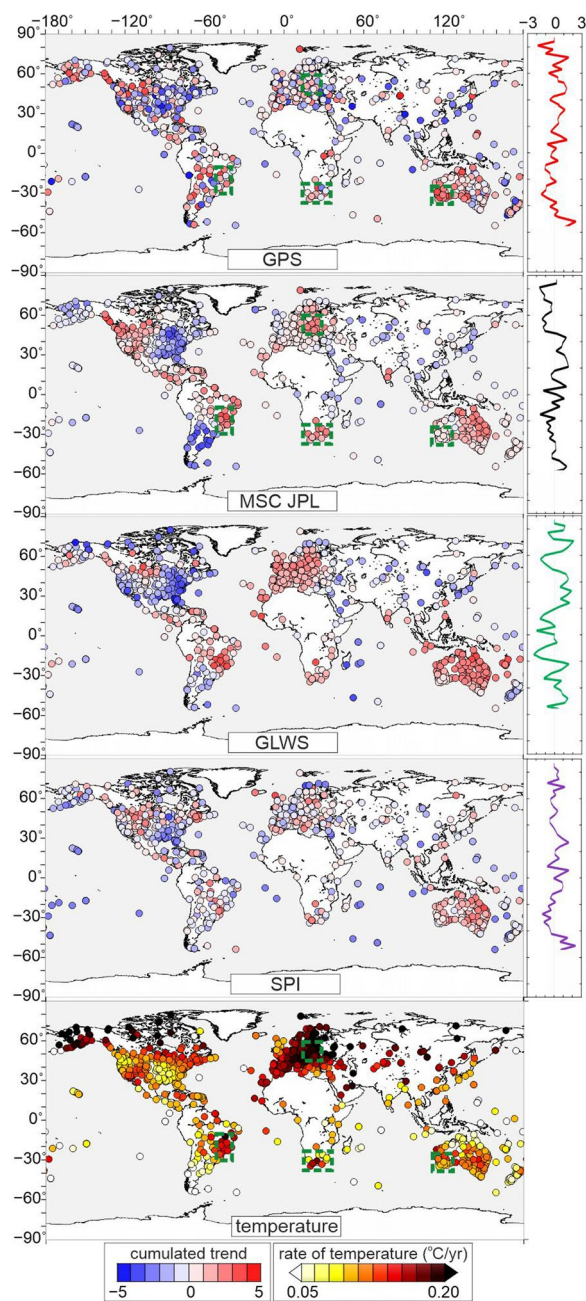


Fig. 6 Map of trend estimated for cumulated DSIs determined for GPS-observed, GRACE-derived, GLWS-predicted vertical displacements and SPI traditional climate index. We used GRACE JPL mascon solutions. The zonal average trend values (right) were determined using smoothing with a 1° moving window. The bottom map presents the rate of global surface temperature in $^\circ\text{C}/\text{yr}$. The green dashed lines in upper map indicate the areas selected to regional analysis discussed in Figs. 7 and 8

for European regions which have been subjected to more intense and more frequent local flash droughts over the past years (Walker et al. 2023). All changes are no

detectable by GRACE causing the differences between trends estimated for GPS-DSI and GRACE-DSI. For example, the lack of significant trends for GRACE-DSI in these regions may be attributed to the dampening effect of GRACE data spatial averaging. Consequently, the results are different and highlight mostly drying conditions for GRACE and GLWS; however, there are wetting conditions for GPS that coincide with SPI results. We further analyze the zonal average trends presented as time series in Fig. 6. In the equatorial region (within 15°N and 15°S latitudes), the wetting trends occur more frequently for each estimated DSIs. However, the wetting trend is observed closer to 15° in northern hemisphere. For the northern mid-latitudes regions (15°N to 50°N), the drying trends are dominated and range from 1 to 2 per year and are clearly dominant for GRACE and GLWS. It agrees with estimated temperature rate over $0.15^\circ\text{C}/\text{yr}$, as observed in the bottom map of Fig. 6. GPS-DSI and SPI indicate some negative values around 40° latitude. For all data, the averaged trend below -1 per year is noted in the southern mid-latitudes. For the higher latitudes, the trends for GPS- and GRACE-DSI are consistent. We observe wetting tendencies for latitudes higher than 50° in southern hemisphere for which temperature rate less than $0.08^\circ\text{C}/\text{yr}$ is registered. The drying trends are found in northern hemisphere rising to the minimum values above 80°S latitude. In the case of SPI, the changing trends are relatively stable in the northern hemisphere and do not follow the significant trend changes estimated from GPS and GRACE. The SPI-derived trends fluctuate around 0 per year.

3.5 Regional analysis

To study regional hydrometeorological changes, we choose regions characterized by extreme climate conditions, i.e., extreme values of estimated DSI cumulated trend and temperature rate (maps in Fig. 6) and regions characterized by the weakest agreement between both geodetic measurements, i.e., different values of estimated DSI cumulated trend (maps in Fig. 6) and low correlation (maps in Fig. 1). We select four regions located in different hemispheres and characterized by different climate conditions: (i) the east parts of Brazil ($10^\circ\text{--}30^\circ\text{S}$ latitude and $40^\circ\text{--}50^\circ\text{W}$ longitude) and (ii) Europe ($45^\circ\text{--}60^\circ\text{N}$ latitude and $15^\circ\text{--}30^\circ\text{E}$ longitude), (iii) the west part of Australia ($28^\circ\text{--}38^\circ\text{N}$ latitude and $115^\circ\text{--}125^\circ\text{E}$ longitude), and (iv) the south part of Africa ($25^\circ\text{--}35^\circ\text{S}$ latitude and $10^\circ\text{--}30^\circ\text{E}$ longitude). First two regions are characterized with DSI cumulated trend over 3 and 2 per year determined from GPS and GRACE, and temperature rate over $0.11^\circ\text{C}/\text{yr}$ and $0.20^\circ\text{C}/\text{yr}$, respectively. The last two regions are characterized with various conditions, i.e., stations within Australian region indicate DSI cumulated

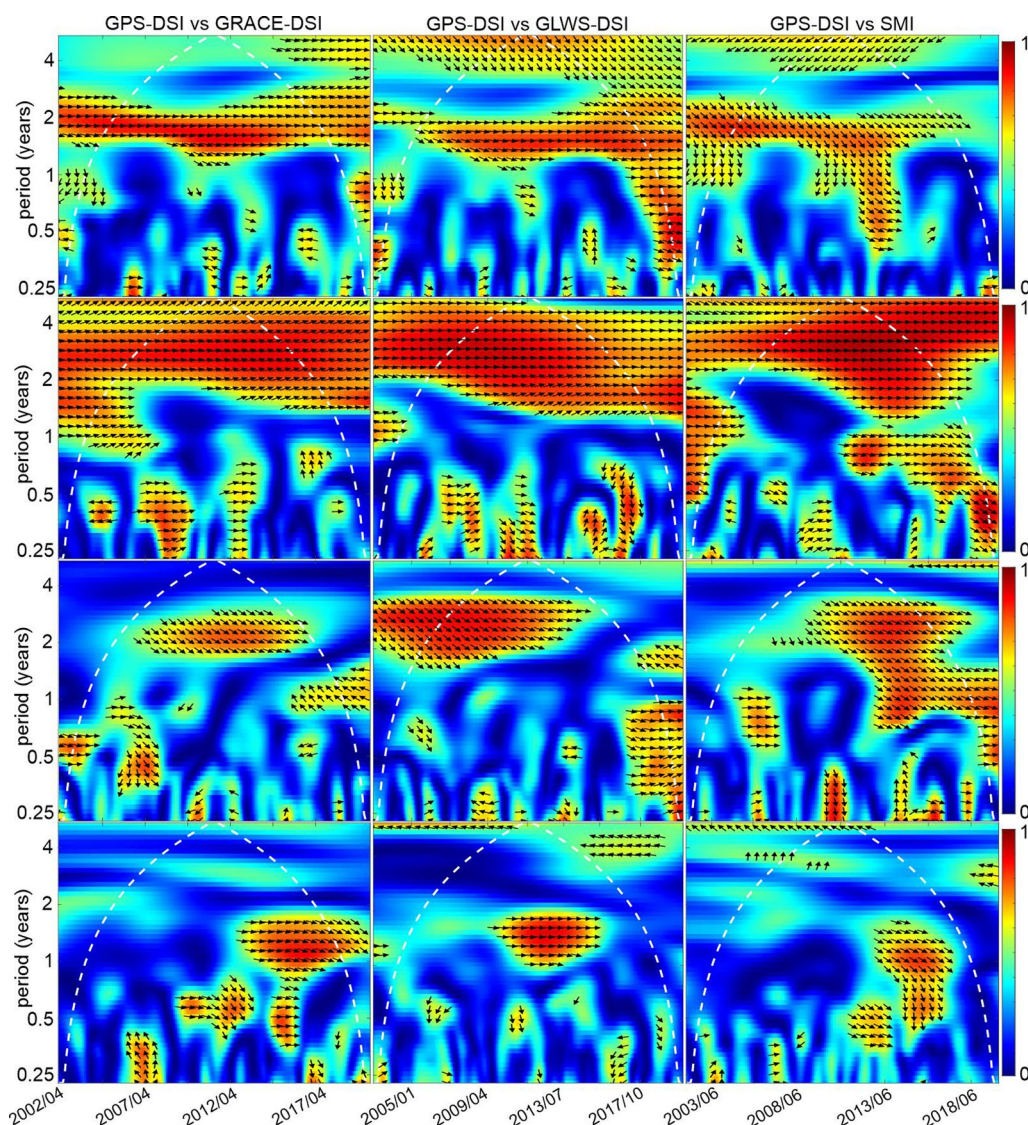


Fig. 7 Wavelet coherence between GPS-DSI and DSI estimated from GRACE JPL mascon solution (left column), GLWS (middle column), and Soil Moisture Index (right column). The rows show the results obtained for the eastern Brazil, the eastern Europe, the western Australia, and the southern Africa regions, respectively, from first to fourth row. Warmer and cooler colors reflect, respectively, the high and low coherence between DSI series. The direction of the arrows specifies a phase relationships between time series where horizontal arrow indicates the same (to right) and opposite (to left) phase. The vertical upward arrows assert that the GPS-DSI is advancing by 90°, and the vertical downward arrows confirm that GPS-DSI is delayed. The dashed white line is the cone of wavelet influence representing the area with greater influence of the wavelet transform edge effect

trend over 3 and near 0 per year determined from GPS and GRACE; however, in African region we note a correlation around 0 between DSI based on GPS and GRACE data.

3.5.1 Wavelet coherence analysis

In Fig. 7, the correlations of GPS-DSI with GRACE-DSI, GLWS-DSI and SMI (respectively, from left to right column) via cross-phase angle and period are presented. In

the case of Brazil region (first row), we find strong consistency between GPS and other drought indices for 1.5 to 3 years signals during 2002–2019 period. The obtained correlation exceeds 0.7. We further observe the intermittent positive coherences (over 0.5) on a short time period of 3–8 months near 2007, 2011, 2013–2014, 2016–2017, and 2018/2019 that are related to droughts recorded in Brazil caused mostly by below-average precipitation (Knowles et al. 2020). We note that GPS- and GRACE/

GLWS-DSIs are in phase (arrows pointing to the right). For SMI, arrows mainly point to the right-down indicate that GPS is advanced by 3 months. It may mean that soil moisture is lag behind meteorological changes monitored by GPS that have been already noticed by Tian et al. (2022) for the Yangtze river basin. However, we note that GLWS-DSI and SMI are strongly correlated with GPS-DSI for long periods in the eastern Brazil for which we obtain relatively stable coherence between 4 year DSI signals. The 4 year signals for GRACE are consist with GPS in 2018–2019, which are not captured by SMI. For European region (second row), we notice significant relationships of GPS-derived and other data on a short time scale up to 9 months. Overall, we obtain coherency of more than 0.6 around 2005, 2008–2009, 2012–2013, 2017–2018 that stems from the heavy rains and rapid temperature variations (Paprotny et al. 2018) that are captured by all used datasets. These time intervals coincide with a sudden DSI decrease or increase by values of 1–2 (Fig. 8). DSI signals are in phase for most of periods, excluding 2017 for GLWS and 2019 for SMI, for which GPS is advancing by 2–3 months. In the following years, i.e., 2018–2019, the normal conditions were recorded in the Eastern Europe, which are indicated by GPS and SMI (correlation over 0.8). GRACE and GLWS overestimate the normal conditions for GPS-DSI by showing (extremely) wet conditions (Fig. 8). We find the strong coherence over 0.6 for signals longer than 2 years for the entire period and for 1.5 year signals since 2011/2012 for all datasets which coincide with regularly appearing extreme dry and wet events recorded in Europe. For example, a high correlation between GPS- and GRACE-DSIs up to 2008 for 1–2 year signals reflects extreme DSI variations related to systematic heatwaves and heavy rains in central and eastern parts of Europe (Zeder and Fischer 2020). For Australian region (third row), we note a strong correlation (over 0.6) between GPS-DSI and other data on a 3- or 4 month signals, even to seasonal. Overall, it is observed around 2002–2003, 2006–2007, 2010 for GRACE-DSI, 2007, 2009, 2013–2014, 2019 for GLWS-DSI and 2006, 2011, 2013–2015, 2019 for SMI. These significant signals stem from a long-term temperature increases (Tangdamrongsub et al. 2021) and coincide with a rapid DSI variations by values up to ± 3 (Fig. 8). For most of periods, GPS is advancing by 3–6 months or is even in the opposite phase with GRACE- and GLWS-DSIs for 2011–2012 period. In the following years GPS is more sensitive than GRACE and GLWS to recorded short-term temperature variations in the western Australia areas (Fig. 8). We notice the high relationships (correlations over 0.7) for 2–4 year signals for 2007–2017, 2003–2015, and 2010–2020 for GRACE-DSI, GLWS-DSI, and SMI, respectively. These period intervals

coincide with regularly appearing extreme dry and wet events recorded in Australia. For GRACE-DSI and SMI, we find coherency for annual signals, respectively, for 2006–2007, 2017–2019, and 2007–2008, 2013–2019 that reflect a rapid DSI decreases and increases related to droughts and regularly heavy rains (Khaki 2020). In the case of South Africa (fourth row), we notice strong consistencies between GPS and GRACE-DSI, GLWS-DSI, SMI for 1 to 2 years signals during 2013–2019, 2010–2016, 2013–2017 periods, respectively, for which correlation exceeds 0.8. We find that GPS- and GRACE-/GLWS-DSIs are in phase; however, GPS is delayed by 2–3 months compared to SMI. We further observe the intermittent positive coherences (over 0.4) on a short time period of 3–9 months in 2007, 2011–2012, 2016, 2017, 2019 for GRACE-DSI, 2007, 2012, 2017 2018 for GLWS-DSI and 2004, 2008, 2011–2014, 2015–2018 for SMI. Those periods relate to droughts and floods recorded in South Africa that are caused mostly by variations in precipitation (Archer et al. 2019). For most of periods, GPS is delayed by 2–4 months, except 2007 and 2004 for which GPS is advanced, and except 2011 and 2008, 2013 for which GPS is in phase with GRACE-DSI and SMI, respectively. The high correlations in the last analyzed years in all data are the result of regular and heavy rainfall in consecutive rainy seasons, since at least 2015 (Almazroui et al. 2020). Those periods are mainly captured by GRACE-DSI and SMI.

3.5.2 Temporal coherence analysis

We next focus on studying the sensitivity of both geodetic techniques to detect hydrometeorological events (Fig. 8). For each region, we estimate a mean DSI series for GPS, GRACE, GLWS, SPI, and SMI datasets. This is performed by estimating a mean signal plus its standard deviation for stations located within each region, showing a spatial variability within the selected region. For eastern Brazil (first graph), from 2004 to 2014, we observe regular variations in temperature, which are captured by all datasets, excluding SPI that underestimates some of them (e.g., 2005, 2007, 2011, 2013, 2016, or 2018). Mostly dominated by longer dry periods than wet ones. After 2014, the precipitation in Brazil region increased (Rodell and Li 2023) and we observe a decline in temperature anomalies that lead to dominant wet events. It is reflected by systematic decrease in DSI values, especially captured by GLWS-DSI. The first three years reflect flash droughts driven mainly by El Niño and rapid Atlantic water warming that led to extreme droughts (Chen et al. 2009) projected clearly by GPS-DSI and SMI. The major drought in 2004 coincides with the rapid 1 °C anomaly temperature increase and is captured by all estimated drought indices. Then there is a

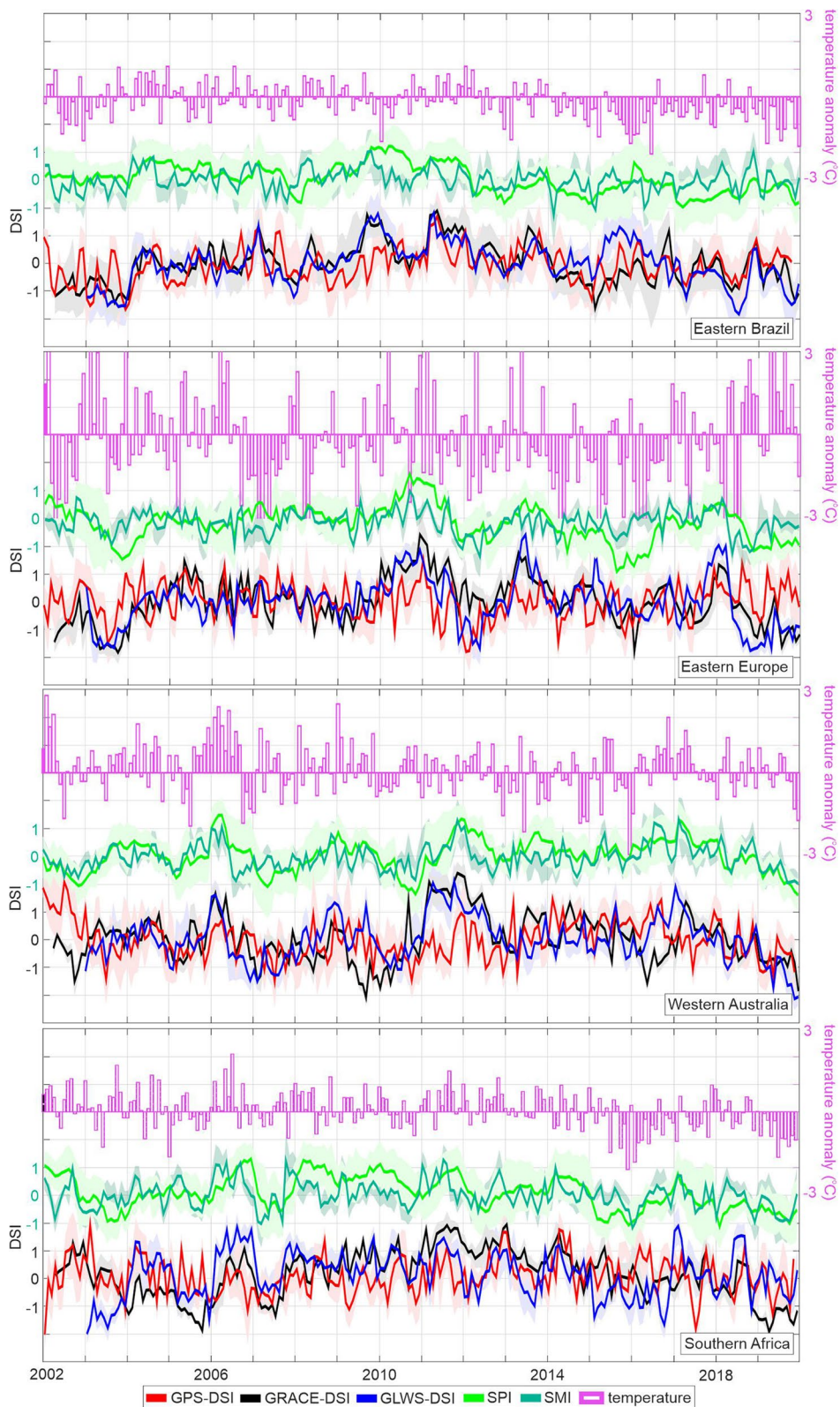


Fig. 8 Time series of DSI determined from GPS-observed, GRACE-derived, GLWS-predicted vertical displacements, and SPI and SMI climate indices for the eastern Brazil, the eastern Europe, the western Australia, and the southern Africa regions, respectively, from first to fourth row. For GRACE determinations, we use JPL mascon solution. The shaded area is understood as a spatial variability within the region. The drought indices are compared with global surface temperature anomalies presented in °C

noticeable decrease in DSIs by 1.5–2 between 2007 and 2010 reflecting a slow recovery from the dry years (Rodell et al. 2018). We note smaller DSI values determined from GPS than GRACE and GLWS that may be related with local wet events occurred in coastal areas. However, they are spatially averaged and underestimated by GRACE and model. Over 2010–2019, we observe a tendency toward more wet conditions with few dry events related with DSI decrease. The significant impact of flooding is found in 2010/2011 and 2011–2015 (Espinoza et al. 2014) that reflects rapid DSI decrease up to 4 (from around +2 to –2) after 2011 determined either from GPS, or GRACE and GLWS. In 2013, the historical unprecedented compound dry and hot conditions were recorded in Brazil (Geirinhas et al. 2022) that are captured as peak by 1.5 in DSI series. Another extreme dry period coincides with a late 2015 major drought (Jiménez-Muñoz et al. 2016) whose impact is seen over the next two years, as reflected by GPS-DSI increases but underestimated by GRACE-DSI. For Europe (second graph), the extreme temperature anomaly ranges ± 3 °C and mostly coincides with recorded periods of dry and wet events. In late 2002, intense rainfall of long duration induced extreme flooding spanning countries of Eastern Europe (Ulbrich et al. 2003) that is captured as decrease by almost 2 in DSI series for GPS and GRACE. SMI detects it as a DSI decrease by 1. Then, heavy rains are monitored in 2013–2014 (Grams et al. 2014) for which we note DSI decreases by 3 for GPS, GRACE, GLWS and by 2 for SMI. In the following years, there are regular long-term changes interrupted by meager rainfall amounts and near-record levels of global temperature anomaly leading to severe drought, subsequent crop loss, or forest fires in 2010–2011 (Spinoni et al. 2015). It is related with the largest GPS- and GRACE-DSI values and DSI rise by 1 and 2, respectively, for SMI and SPI. The anomaly temperature also peaks to 3 °C. In 2012, we notice DSI decrease by 4 for SMI and by 3 for SPI that reflect the widespread flooding after a wave of heavy rains (Spinoni et al. 2015). It is coincided with observed 2 to 3 °C temperature declines. The year 2013 is characterized with normal conditions with short-term increased amounts of rainfall for the last few months (Grams et al. 2014). While these conditions are effectively captured by GPS-DSI and SMI, however, they are overestimated by DSIs estimated from GRACE and GLWS. In next years, a large area of south-eastern and central parts of Europe was affected by cyclone causing floods and landslides, which are captured either by GPS-DSI and SPI. In 2018 and 2019, extremely dry conditions with anomaly temperatures exceeding 2 °C are registered across mainly central and eastern parts of Europe (Blauhut et al. 2022). Both events are captured only by GPS as a DSI increase by almost 2.

Nevertheless, 2019 drought is also noticed by SMI and SPI series as index increase of 1. In the case of Australia (third) and Africa (fourth) regions, the poor correlation between both geodetic measurements may come from the weak concordance of long-term signals (more than a year) presented in Fig. 7. However, in Australia, we note that GPS and GRACE are characterized by a good temporal consistency with other datasets, especially during extreme hydrometeorological events. We observe similar changes in several periods (e.g., 2005, 2006–2009, 2009–2010, 2011–2012, 2016–2017), which correspond to peaks in time series representing extreme conditions recorded in the west part of continent. Those periods coincide with extreme droughts described by Wang et al. (2021), which are detected as a DSI increase by at least 2 for all used data. For example, during 2006–2009 period the prolonged severe drought is recorded in Mainland Australia affecting over 60% of continent areas. It is observed by both GPS and GRACE, coinciding with DSIs values over 1.5 and temperature up to 3 °C lasting 1.5 year. The significant variations in 2011 and 2016 reflect the impact of both ENSO and the Indian Ocean Dipole (IOD) events on the hydrological droughts (Ferooatan et al. 2019). SPI and SMI detect these variations as a DSI increase by 1–2. The extreme dry conditions in 2011 are effectively captured by DSIs estimated from GRACE, GLWS, SPI and SMI. However, GPS-DSI indicates moderate conditions in 2011 underestimating the index value. For 2016, GRACE-DSI series do not capture dry conditions pointing to wet ones. Then, heavy rains are monitored in 2005, 2009–2010 (Ferooatan et al. 2019) for which we note DSI decreases by 2–3 for GPS, GRACE, GLWS and by 1 for SPI and SMI. In the following years, there are regular near seasonal changes interrupted by moderate rainfall amounts and high global temperature anomaly. It is related with DSI ranging between –1 and 1.5 and between –1 and 1 for both SMI and SPI climate indices, respectively. The temperature anomaly ranges ± 1.5 °C. The systematically DSI decrease in the last 3 analyzed years is driven mainly by rainfall in consecutive rainy seasons (Wang et al. 2021), which is effectively captured by GPS, GRACE, and GLWS; however, it is underestimated by SPI and SMI. Finally, in 2019 we observe the temperature anomaly ranges ± 1 °C and significantly DSI decreases indicating Australian flash flood (Liu et al. 2020). For the selected southern Africa region (fourth graph), from 2002 to 2015, we observe the dominance of the positive temperature anomaly reflecting mostly dry conditions ($DSI > 0$) by all datasets (e.g., 2002/2003, 2004, 2006, 2008, 2010, 2011, 2012/2013 and 2014) confirming drought periods described by Malherbe et al. (2016) using SPI. Most of them show extreme conditions. Some of the periods such as 2004, 2006 and 2010, 2011 are

underestimated by, respectively, GRACE and GPS compare to literature. The first five years reflect exceptional droughts driven mainly by rapid decrease in precipitation (Hastenrath et al. 2017) projected clearly by all DSI series as DSI decrease by 2. These periods coincide with temperature increase up to 2 °C. Droughts are interrupted by heavy rains recorded in 2003, 2005, and 2007 (Vogel et al. 2010) that are picked up by all estimated drought indices. However, GLWS overestimates conditions monitored by both geodetic-derived DSIs and climate indices in 2003. Furthermore, we note smaller DSI values determined from GRACE than GRACE and GLWS. It may be related with GRACE data spatial resolution that is smaller than other data. For all wet periods, DSI decreases coincide with short-period temperature declines ranging from –2 to –1 °C. Then there is a noticeable decrease in DSIs by up to 2 during 2015 extreme drought. The negative DSI values even though droughts reflect a crust poroelastic response to groundwater pumping within sedimentary basin (Bonsor et al. 2018). Then, in spite of a temperature of around –3 °C in 2016 we find dry conditions indicating the most intense drought event caused by the El Niño over Southern Africa associated with a pronounced dipole of opposing rainfall anomalies (Kolusu et al. 2019). This event is underestimated by GRACE and GLWS, and is not captured by SPI and SMI. The significant impact of flooding is found in 2018/2019 (Scanlon et al. 2022) that reflects rapid DSI decrease up to 3 after mid-2018 determined either from GPS, GRACE and GLWS. It coincides with SPI and SMI decreases by 1–1.5 and temperature anomalies around –1 °C with maximum –1.5 °C in 2019.

The results obtained for both GPS and GRACE techniques are coherent at different frequencies as well. The decomposed signals (Fig. A4, A5) show good temporal agreement for short-term, seasonal and long-term signals. For example, the significant DSI changes in short-term signals indicate extreme hydrometeorological events for both GPS and GRACE series. The estimated seasonal changes are time-coherent with regional interannual hydrological changes. Further, we find consistent multi-year variations between GPS- and GRACE-DSIs that overlap with ENSO signals for the long-term component.

To further highlight the potential of geodetic measurements to study regional hydrometeorological changes, in Figure A3 we also present the DSI time series estimated using GPS-observed, GRACE-derived, GLWS-predicted vertical displacements, and SPI and SMI traditional climate indices for the ten river basins (Fig. A2). We choose the river basins by reference to basins indicated as the major to study water availability by Lakshmi et al. (2018) that cover the largest area (Scanlon et al. 2016). The river basin shapes are downloaded from the Food

and Agricultural Organization of the United Nations (FAO-UN). We additionally assume the requirement of availability of (at least 3) GPS stations. Finally, we show basins on all continents, excluding Africa, for which an appropriate number of stations are available only for the Orange river basin. (We have been already discussed the results for Orange river in Figs. 7, 8 as south part of Africa region.) The results for the selected basins show the strong temporal coherence between geodetic-derived DSIs and other drought indices. We identify the advantages of the determined indices to detect and analyze dry and wet events, as can be verified by comparing our results with those shown in previous literature (e.g., Scanlon et al. 2016, 2018; Ferreira et al. 2023; Tangdamrongsub 2023; Zhong et al. 2023).

4 Summary and conclusions

We study GPS- and GRACE-DSI series based on ground displacements estimated for 999 GPS locations spread across the world. For GRACE-type data, we analyze both spherical harmonics and mascon solutions provided by two different processing centers. The obtained results are compared with traditional climate indices and temperature. For detailed discussion, we select four regions located in both hemispheres and characterized with various hydroclimatic variability, i.e., the east parts of South America and Europe, the west part of Australia, and the south part of Africa.

The global study highlights strong temporal and spatial coherence between GPS- and all GRACE-DSIs. We find concordance correlation coefficient values greater than 0.5 for at least 30% of stations, while over 80% of them are positively correlated. The largest concordance is observed for both Americas and Europe, mainly in central continental areas. In the case of climate zones, the strong correlated regions occur in continental and temperate zones. They overlap with the regions characterized by extreme TWS trends (e.g., central US or southern Brazilian regions) and annual amplitudes (e.g., Amazon river basin, eastern Africa, or southern European regions). The negatively correlated stations are mostly spread over island and coastal areas. Similar results we obtain for variance reduction parameter for which the positive values are found at 91% of stations for both type of GRACE data. The poor agreement is observed along the coastal areas and in Western Australia. For the central parts of North America, Brazil, and southern parts of Europe, we indicate the strongest agreement in DSIs annual amplitude and phase between GPS and all GRACE data. The climate zones analysis indicates the increasing correlation values correspond to decreasing RMS of DSI differences for which the slopes of linear relationships range from –0.9 to –0.7. The smallest slope value is found for

tropical climate zone; however, it is almost twice as large for continental zone.

We indicate the significant resemblance for DSI based on GRACE data provided by two different processing centers. The even better (temporal and spatial) agreement with GPS is observed for both JPL and CSR mascons for which the median values are 0.1 greater than for spherical harmonics. DSI based on mascons are also characterized with better phase and amplitude agreement with GPS-DSI. The seasonal variations in DSIs are similar for all GRACE data. For example, almost 75% of stations are characterized with amplitude of DSI difference smaller than 0.5 with median up to 0.2.

The results obtained using traditional climate indices demonstrate that GPS-DSI coincides with SPI and SMI. We notice similar temporal changes at 85% of stations for GPS-DSI and both traditional indices. We find correlation greater than 0.5 for more than 40% of stations. The weakly correlated areas are noticed mostly at middle latitudes, e.g., Latin America, the central part of Asia, and island areas. Moreover, there are two major similarities for individual climate zones i.e., (i) 50% of stations are characterized with anomalies greater than 0.5 for both SPI and SMI for the (semi-)arid zone, and (ii) the lowest agreement is observed in continental zone for which correlations exceeding 0.5 are found for SPI for only 6% more stations than for SMI. We show that GPS- and GRACE-DSIs are characterized with similar drought characteristics as obtained using GLWS-DSI and temporally coherent with temperature anomalies. For example, we find that 9 month droughts dominate for all three datasets and are observed at least 72% of stations. The shorter droughts are mostly found in island areas or even in coastal areas for GPS. We indicate the average length of drought near 12, 14, and 15 months for GPS-, GRACE-, and GLWS-DSI, respectively. Droughts longer than 1 year occur in a nearly unbroken belt around the Earth at low latitudes, mostly within 15° in both hemispheres. In the case of drought category, we notice that moderate conditions dominate for all climate zones for which drying conditions are observed for at least 40% of all analyzed months. We need to point out that results we obtain indicate an increase in the number of dry events in the second half of analyzed period, while the number of wet events has been consistently decreasing. We find that at least 52% of stations are characterized with positive DSI cumulated trend and coincide with regions characterized by temperature rates over 0.1 °C/yr and drying hot spots indicated by Jensen et al. (2019).

Our regional drought indices analysis highlights that DSI based on geodetic measurements are even more sensitive to monitor and detect physical hydrometeorological events than traditional climate indices. It is pointed out

by studying the variation in DSI values in the recorded dry and wet events occurring in Brazil, Europe, Australia, and Africa areas. For example, we find strong consistency between GPS-DSI and GRACE-DSI/GLWS-DSI/SMI for long- (i.e., 1.5 to 3 years) and short-term (i.e., 3 to 8 months) signals in Brazil that are related to dry periods. The analyzed drought indices estimated from GPS, GRACE, GLWS are mostly in phase; however, GPS-DSI is led by 3 months in comparison with SMI. For Europe, DSI series are in phase for most of extreme periods and are characterized with strong relationships on a short and a long time scale, respectively, up to 9 months and over 2 years. In the case of Australian region, we note a correlation over 0.6 between GPS-derived and other data on a 3 or 4 months signals, even to seasonal. These signals stem from a short-period temperature increases and coincide with a rapid DSI variations by values up to ± 3 . For most of periods, GPS is advancing by 3–6 months or is even in the opposite phase with GRACE- and GLWS-DSIs for 2011–2012 period. For South Africa, we notice a strong consistency between GPS and the estimated drought indices for 1 to 2 years signals during at least 6 year periods, for which correlation exceeds 0.8. GPS- and GRACE-/GLWS-DSIs are mostly in phase. However, GPS is delayed by 2–3 months compare to SMI. Further, we highlight that GPS-DSI is characterized by a large level of consistency with GRACE-DSI signals at different temporal scales estimated using nonparametric wavelet decomposition (Fig. A4, A5). We note the sensitivity of short-term signals to extreme hydrometeorological events, the seasonal to interannual hydrological changes, and multi-year variations coincided with ENSO signals for the long-term component for both GPS- and GRACE-DSI series.

The following analysis highlights that adopting the geodetic techniques to drought analysis is a notable step toward improving the reliability of extreme events detection in the context of local and regional studies. GPS and GRACE indicate the ability to detect hydroclimatic and hydrometeorological changes for both long- and short-term scales, even better than traditional climate indices since traditional climate indices underestimate or are not able to capture recorded extreme events. It is also well illustrated in the selected ten river basins shown in Figure A2, A3 in Online Appendix. The strong amplitude and phase agreement between geodetic-derived DSIs with temperature anomalies, hydrological model, etc. increase the ability for enhancing our understanding of evolving drought characteristics (e.g., patterns, occurrences, category, duration) providing a synoptic insight of processes related with water mass variations. That may be essential for affording vital information for understanding climate changing and efficiently managing

water resources. Our research highlights the challenges and benefits of using traditional climate indices and geodetic measurements across global and regional scales. These insights are crucial for accurately interpreting localized analyses such as point-wise analyses. The present study provides a strong background to many (future) researches that are based on various drought indices and the assessment of their reliability.

Abbreviations

CCI	Climate Change Initiative
CLSM	Catchment Land Surface Model
CSR	Center for Space Research
DSI	Drought Severity Index
ENSO	El Niño Southern Oscillation
ERA5	European Centre for Medium-Range Weather Forecasting Atmospheric Reanalysis
ESA	European Space Agency
ESM GFZ	Earth System Modelling Group of Deutsches GeoForschungsZentrum
FAO-UN	Food and Agricultural Organization of the United Nations
GISTEMP	GISS Surface Temperature Analysis
GPCC	Global Precipitation Climatology Centre
GLWS	Global Land Water Storage
GNSS	Global Navigation Satellite System
GPS	Global Positioning System
GRACE	Gravity Recovery and Climate Experiment
IGS	International GNSS Service
IOD	Indian Ocean Dipole
IQR	Inter-Quartile Range
JPL	Jet Propulsion Laboratory
MODIS	Moderate Resolution Imaging Spectroradiometer
NGL	Nevada Geodetic Laboratory
NOAA	National Oceanic and Atmospheric Administration
NAO	North Atlantic oscillation
PDO	Pacific Decadal Oscillation
PDSI	Palmer Drought Severity Index
PPP	Precise Point Positioning
RMS	Root mean square
SLR	Satellite Laser Ranging
SMI	Soil Moisture Index
SPI	Standardized Precipitation Index
SPEI	Standardized Precipitation Evapotranspiration Index
SWSI	Surface Water Supply Index
TWS	Total Water Storage
WaterGAP	Water-Global Assessment and Prognosis
WGHM	WaterGAP Global Hydrological Model

Supplementary Information

The online version contains supplementary material available at <https://doi.org/10.1186/s40645-024-00665-4>.

Supplementary file 1.

Acknowledgements

Maps are generated using the Generic Mapping Tools software (Wessel et al. 2019).

Author contributions

Conceptualization was performed by AL, LOG, AK, JB; data curation by AL, AK, JB; formal analysis by AL, LOG; funding acquisition by AL, LOG, AK, JB; investigation by AL; methodology by AL; project administration by AL, LOG, AK, JB; resources by AL, AK, JB; software by AL; supervision by LOG, AK, JB; validation by AL, LOG; visualization by AL; roles/writing—original draft by AL; writing—review & editing by AL, LOG, AK, JB.

Funding

AL, AK, and JB are funded from the Military University of Technology, Faculty of Civil Engineering and Geodesy. Also this work was partially supported by the European project, CORSO (grant agreement 101082194), by the European Space Agency (ESA) as part of the ESA Climate Change Initiative (CCI), and by the French National Space Agency (CNES) TOSCA projects through the funding of LOG.

Availability of data and materials

GPS data are available through: <http://geodesy.unr.edu/> for NGL solutions. GRACE/-FO mascon solution is available on: http://www2.csr.utexas.edu/grace/RL06_mascons and https://grace.jpl.nasa.gov/data/get-data/jpl_global_mascons/ websites, respectively, for CSR and JPL centers. GRACE/-FO spherical harmonics coefficients are provided at: <http://icgem.gfz-potsdam.de/sl/temporal> website. Traditional climate indices SPI and SMI are available through: <https://edo.jrc.ec.europa.eu/>. The temperature data are downloaded from: <https://data.giss.nasa.gov/>.

Declarations

Competing interests

The authors declare that they have no competing interest.

Received: 21 May 2024 Accepted: 3 November 2024

Published online: 02 December 2024

References

- Almazroui M, Saeed F, Saeed S, Nazrul Islam M, Ismail M, Klutse NAB, Sddiqui MH (2020) Projected change in temperature and precipitation over Africa from CMIP6. *Earth Syst Environ* 4:55–475. <https://doi.org/10.1007/s41748-020-00161-x>
- Archer E, Landman W, Malherbe J, Taddross M, Pretorius S (2019) South Africa's winter rainfall region drought: a region in transition? *Clim Risk Manage* 25:100188. <https://doi.org/10.1016/j.crm.2019.100188>
- Argus DF, Fu Y, Landerer FW (2014) Seasonal variation in total water storage in California inferred from GPS observations of vertical land motion. *Geophys Res Lett* 41:1971–1980. <https://doi.org/10.1002/2014gl059570>
- Azad MAK, Towfiqul Islam AR, Ayen K, Rahman S, Shahid S, Mallick J (2022) Changes in monsoon precipitation patterns over Bangladesh and its teleconnections with global climate. *Theor Appl Clim* 148(3–4):1261–1278. <https://doi.org/10.1007/s00704-022-03996-8>
- Bettadpur S (2018) GRACE (GRACE 327-742 (CSR-GR-12-xx)) (gravity recovery and climate experiment follow-on), UTCSR level-2 processing standards document (Rev. 5.0, April 18, 2018), (For Level-2 Product Release 0006), Center for Space Research, The University of Texas at Austin
- Bhanja SN, Mukherjee A, Rangarajan R, Scanlon BR, Malakar P, Verma S (2019) Long-term groundwater recharge rates across India by in situ measurements. *Hydro Earth Syst Sci* 23(2):711–722. <https://doi.org/10.5194/hess-23-711-2019>
- Blauhut V, Stoezle M, Ahopelto L, Brunner MI, Teutschbein C, Wendt DE, Aktinas V, Bakke SJ, Barker LJ, Bartošová L, Briede A, Cammalleri C, Kalin KC, De Stefano L, Fendeková M, Finger DC, Huysmans M, Ivanov M, Jaagus M, Jakubinský J, Krakovska S, Laaha G, Lakatos M, Manevski K, Andersen MN, Nikolova N, Osuch M, van Oel P, Radeva K, Romanowicz RJ et al (2022) Lessons from the 2018–2019 European droughts: a collective need for unifying drought risk management. *Nat Hazards Earth Syst Sci* 22:2201–2217. <https://doi.org/10.5194/nhess-22-2201-2022>
- Blewitt G, Hammond WC, Kreemer C (2018) Harnessing the GPS data explosion for interdisciplinary science. *Eos* 99. <https://doi.org/10.1029/2018E0104623>
- Bonsor H, Shamsudduha M, Marchant B, MacDonald A, Taylor R (2018) Seasonal and decadal groundwater changes in African sedimentary aquifers estimated using GRACE products and LSM. *Remote Sens* 10:904. <https://doi.org/10.3390/rs10060904>
- Cammalleri C, Vogt JV, Bisselink B, de Roo A (2017) Comparing soil moisture anomalies from multiple independent sources over different regions

- across the globe. *Hydro Earth Sys Sci* 21(12):6329–6343. <https://doi.org/10.5194/hess-21-6329-2017>
- Chen J, Wilson C, Tapley B, Yang ZL, Niu GY (2009) 2005 drought event in the Amazon river basin as measured by GRACE and estimated by climate models. *J Geophys Res Solid Earth*. <https://doi.org/10.1029/2008JB006056>
- Cui D, Liang S, Wang D, Liu Z (2021) A 1-km global dataset of historical (1979–2017) and future (2020–2100) Köppen-Geiger climate classification and bioclimatic variables. *Earth System Science Data*. <https://doi.org/10.5194/essd-2021-186>
- Dai A (2013) Increasing drought under global warming in observations and models. *Nat Clim Chang* 3(1):52–58. <https://doi.org/10.1038/nclimate1633>
- Dill R, Dobslaw H (2013) Numerical simulations of global-scale high-resolution hydrological crustal deformations. *J Geophys Res Solid Earth* 118(9):5008–5017. <https://doi.org/10.1002/jgrb.50353>
- Eriyagama N, Smakhtin V, Gamage N (2009) Mapping drought patterns and impacts: a global perspective. Colombo, Sri Lanka: International Water Management Institute. p.31 IWMI research report at http://www.iwmi.cgiar.org/Publications/IWMI_Research_Reports/PDF/PUB133/RR133.pdf.
- Espinoza JC, Marengo JA, Ronchail J, Carpio JM, Flores LN, Guyot JL (2014) The extreme 2014 flood in southwestern Amazon basin: the role of tropical-subtropical south Atlantic SST gradient. *Environ Res Lett* 9(12):124007. <https://doi.org/10.1088/1748-9326/9/12/124007>
- Farrell WE (1972) Deformation of the Earth by surface loads. *Rev Geophys Space Phys* 10(3):761–797. <https://doi.org/10.1029/RG010i003p00761>
- Ferreira V, Ndehedehe ChE, Montecino HC, Yong B, Yuan P, Abdalla A, Mohamed A (2019) Prospects for imaging terrestrial water storage in south america using daily GPS observations. *Remote Sens* 11(6):679. <https://doi.org/10.3390/rs11060679>
- Ferreira V, Yong B, Montecino H, Ndehedehe ChE, Seitz K, Kutterer H, Yang K (2023) Estimating GRACE terrestrial water storage anomaly using an improved point mass solution. *Sci Data* 10:234. <https://doi.org/10.1038/s41597-023-02122-1>
- Forootan E, Khaki M, Schumacher M, Wulfmeyer V, Mehrnegar N, van Dijk AJM, Brocca L, Farzaneh S, Akinluyi F, Ramillien G, Shum CK, Awange J, Mostafaie A (2019) Understanding the global hydrological droughts of 2003–2016 and their relationships with teleconnections. *Sci Total Environ* 650:2587–2604. <https://doi.org/10.1016/j.scitotenv.2018.09.231>
- Fu Y, Argus DF, Landerer FW (2015) GPS as an independent measurement to estimate terrestrial water storage variations in Washington and Oregon. *J Geophys Res Solid Earth* 120(1):552–566. <https://doi.org/10.1002/2014JB011415>
- Gaspar P, Wunsch C (1989) Estimates from altimeter data of barotropic Rossby waves in the northwestern Atlantic Ocean. *J Phys Oceanogr* 19:1821–1844. <https://doi.org/10.1175/1520-0485>
- Geirinhas JL, Russo AC, Libonati R, Miralles DG, Sousa PM, Wouters H, Trigo RM (2022) The influence of soil dry-out on the record-breaking hot 2013/2014 summer in Southeast Brazil. *Sci Rep* 12:5836. <https://doi.org/10.1038/s41598-022-09515-z>
- Gerdener H, Engels O, Kusche J (2020) A framework for deriving drought indicators from the gravity recovery and climate experiment (GRACE). *Hydro Earth Sys Sci* 24(1):227–248. <https://doi.org/10.5194/hess-24-227-2020>
- Gerdener H, Kusche J, Schulze K, Döll P, Klos A (2023) The global land water storage data set release 2 (GLWS2.0) derived via assimilating GRACE and GRACE-FO data into a global hydrological model. *J Geod* 97:73. <https://doi.org/10.1007/s00190-023-01763-9>
- Grams CM, Binder H, Pfahl S, Piaget N, Wernli H (2014) Atmospheric processes triggering the central European floods in June 2013. *Nat Hazards Earth Syst Sci* 14:1691–1702. <https://doi.org/10.5194/nhess-14-1691-2014>
- Gu G, Adler RF (2023) Observed variability and trends in global precipitation during 1979–2020. *Clim Dyn* 61:131–150. <https://doi.org/10.1007/s00382-022-06567-9>
- Han S-C (2017) Elastic deformation of the Australian continent induced by seasonal water cycles and the 2010–2011 La Niña determined using GPS and GRACE. *Geophys Res Lett* 44(6):2763–2772. <https://doi.org/10.1002/2017gl072999>
- Hansen JE, Lebedeff S (1987) Global trends of measured surface air temperature. *J Geophys Res* 92:13345–13372. <https://doi.org/10.1029/JD092iD11p13345>
- Hastenrath S, Polzin D, Mutai Ch (2017) Diagnosing the 2005 drought in equatorial East Africa. *J Clim* 20(18):4628–4637. <https://doi.org/10.1175/JCLI4238.1>
- Huang B, Thorne PW, Banzon VF, Boyer T, Chepurin G, Lawrimore JH, Menne MJ, Smith TM, Vose RS, Zhang H-M (2017) Extended reconstructed sea surface temperature, version 5 (ERSSTv5): upgrades, validations, and intercomparisons. *J Clim* 30(20):8179–8205. <https://doi.org/10.1175/JCLI-D-16-0836.1>
- Jain VK, Pandey RP, Jain MK, Byun H-R (2015) Comparison of drought indices for appraisal of drought characteristics in the Ken River Basin. *Weather Clim Ext* 8:1–11. <https://doi.org/10.1016/j.wace.2015.05.002>
- Jensen L, Eicker A, Dobslaw H, Stacke T, Humphrey V (2019) Long-term wetting and drying trends in land water storage derived from GRACE and CIMP5 models. *J Geophys Res Atmos* 124(17–18):9808–9823. <https://doi.org/10.1029/2018jd029989>
- Jiménez-Muñoz J, Mattar C, Barichivich J, Santamaria-Artigas A, Takahashi K, Malhi Y, Sobrino JA, van der Schrier G (2016) Record-breaking warming and extreme drought in the Amazon rainforest during the course of El Niño 2015–2016. *Sci Rep* 6:33130. <https://doi.org/10.1038/srep33130>
- Khaki M (2020) Efficient assimilation of GRACE TWS into hydrological models. In: Satellite remote sensing in hydrological data assimilation. Springer, Cham. https://doi.org/10.1007/978-3-030-37375-7_6.
- Klos A, Kusche J, Leszczuk G, Gerdener H, Schulze K, Lenczuk A, Bogusz J (2023) Introducing the idea of classifying sets of permanent GNSS Stations as Benchmarks for hydrogeodesy. *J Geophys Res Solid Earth* 128(9):026988. <https://doi.org/10.1029/2023JB026988>
- Knappe E, Bendick R, Martens HR, Argus DF, Gardner WP (2019) Downscaling vertical GPS observations to derive watershed-scale hydrologic loading in the northern rockies. *Water Resour Res* 55(1):391–401. <https://doi.org/10.1029/2018WR023289>
- Knowles LA, Bennett RA, Harig C (2020) Vertical displacements of the Amazon basin from GRACE and GPS. *J Geophys Res Solid Earth*. <https://doi.org/10.1029/2019JB018105>
- Kolusu SR, Shamsudduha M, Todd MC, Tylor RG, Seddon D, Kashaigili JJ, Ebrahim GY, Cuthbert MO, Sorenson JPR, Villholth KG, MacDonald AM, MacLeod DA (2019) The El Niño event of 2015–2016: climate anomalies and their impact on groundwater resources in East and Southern Africa. *Hydro Earth Sys Sci* 23:1751–1762. <https://doi.org/10.5194/hess-23-1751-2019>
- Kottek M, Grieser J, Beck C, Rudolf B, Rubel F (2006) World map of Köppen-Geiger climate classification updated. *Meteorol Z* 15:259–263. <https://doi.org/10.1127/0941-2948/2006/0130>
- Kronland-Martinet R, Molet J, Grossmann A (1987) Analysis of sound patterns through wavelet transforms. *Int J Pattern Recognit Artif Intell* 2:97–126
- Lakshmi V, Fayne J, Bolten J (2018) A comparative study of available water in the major river basins of the world. *J Hydro* 567:510–532. <https://doi.org/10.1016/j.jhydrol.2018.10.038>
- Lenczuk A, Weigelt M, Kosek W, Mikocki J (2022) Autoregressive reconstruction of total water storage within GRACE and GRACE follow-on gap period. *Energies* 15(13):4827. <https://doi.org/10.3390/en15134827>
- Lenczuk A, Klos A, Bogusz J (2023) Studying spatio-temporal patterns of vertical displacements caused by groundwater mass changes observed with GPS. *Rem Sens Environ* 292:113597. <https://doi.org/10.1016/j.rse.2023.113597>
- Lenssen N, Schmidt G, Hansen J, Menne M, Persin A, Ruedy R, Zyss D (2019) Improvements in the GiSTEMP uncertainty model. *J Geophys Res Atmos* 124(12):6307–6326. <https://doi.org/10.1029/2018JD029522>
- Lin LK (1989) A concordance correlation coefficient to evaluate reproducibility. *Biometrics* 45:255–268
- Liu DL, Teng J, Ji F, Anwar MR, Feng P, Wang B, Li L, Waters C (2020) Characterizing spatiotemporal rainfall changes in 1960–2019 for continental Australia. *Int J Clim* 41(S1):E2420–E2444. <https://doi.org/10.1002/joc.6855>
- Malherbe J, Dieppois B, Maluleke P, Van Staden M, Pillay DL (2016) South African droughts and decadal variability. *Nat Hazards* 80:657–681. <https://doi.org/10.1007/s11069-015-1989-y>
- Mao Y, Wu Z, He H, Lu G, Xu H, Lin Q (2017) Spatio-temporal analysis of drought in a typical plain region based on the soil moisture anomaly

- percentage index. *Sci Total Environ* 576:752–765. <https://doi.org/10.1016/j.scitotenv.2016.10.116>
- Materna K, Feng L, Lindsey EO, Hill EM, Ahsan A, Alam AKMK, Oo KM, Than O, Aung T, Khian SN, Bürgmann R (2020) GNSS characterization of hydrological loading in South and Southeast Asia. *Geophys J Int* 224(3):1742–1752. <https://doi.org/10.1093/gji/ggaa500>
- McKee TB, Doesken NJ, Kleist J (1993) The relationship of drought frequency and duration of time scales. In: Eighth conference on applied climatology. American Meteorol Soc 17–23, 179–186.
- Meza I, Siebert S, Döll P, Kusche J, Herbert C, Rezaei H, Nouri H, Gerdener H, Popat E, Frischen J, Naumann G, Vogt JV, Walz Y, Sebesvari Z, Hagenlocher M (2020) Global-scale drought risk assessment for agricultural systems. *Nat Haz Earth Sys Sci* 20(2):695–712. <https://doi.org/10.5194/nhess-20-695-2020>
- Milliner C, Materna K, Bürgmann R, Fu Y, Moore AW, Bekaert D, Adhikari S, Argus DF (2018) Tracking the weight of Hurricane Harvey's stormwater using GPS data. *Sci Adv* 4(9):eaau2477. <https://doi.org/10.1126/sciadv.aau2477>
- Niu G-Y, Yang Z-L (2006) Assessing a land surface model's improvements with GRACE estimates. *Geophys Res Lett* 33:L07401. <https://doi.org/10.1029/2005GL025555>
- Ouellette KJ, de Linage C, Famiglietti JS (2013) Estimating snow water equivalent from GPS vertical site-position observations in the western United States. *Water Resour Res* 49:2508–2518. <https://doi.org/10.1002/wrcr.20173>
- Palmer WC (1965) Meteorological drought
- Paprotny D, Sebastian A, Morales-Nápoles O, Jonkman SN (2018) Trends in flood losses in Europe over the past 150 years. *Nat Commun* 9:1985. <https://doi.org/10.1038/s41467-018-04253-1>
- Peidou A, Argus DF, Landerer FW, Wiese DN, Ellmer M (2023) GPS displacement dataset for study of elastic surface mass variations. *Earth Syst Sci Data Discuss* 16(3):1317–1332. <https://doi.org/10.5194/essd-16-1317-2024>
- Pfeffer J, Cazenave A, Barnoud A (2021) Analysis of the interannual variability in satellite gravity solutions: impact of climate modes on water mass displacements across continents and oceans. *Clim Dyn* 58:1065–1084. <https://doi.org/10.1007/s00382-021-05953-z>
- Qiu J (2010) China drought highlights future climate threats. *Nature* 465:142–143. <https://doi.org/10.1038/465142a>
- Řehoř J, Trnka M, Brázdil R, Fischer M, Bialek J, van der Schrier G, Feng S (2023) Global hotspots in soil moisture-based drought trends. *Environ Res Lett* 19:014021. <https://doi.org/10.1088/1748-9326/ad0f01>
- Ries J, Bettadpur S, Eanes R, Kang Z, Ko U-D, McCullough Ch, Nagel P, Pie N, Poole S, Richter T, Save H, Tapley B (2016) The combined gravity model GGM05C. GFZ Data Services. <https://doi.org/10.5880/icgem.2016.002>
- Rodell M, Li B (2023) Changing intensity of hydroclimatic extreme events revealed by GRACE and GRACE-FO. *Nature Water*. <https://doi.org/10.1038/s44221-023-00040-5>
- Rodell M, Famiglietti JS, Wiese DN, Reager JT, Beaudoing HK, Landerer FW, Lo M-H (2018) Emerging trends in global freshwater availability. *Nature* 557:651–659. <https://doi.org/10.1038/s41586-018-0123-1>
- Save H, Bettadpur S, Tapley BD (2016) High-resolution CSR GRACE RL05 mascons. *J Geophys Res Solid Earth* 121(10):7547–7569. <https://doi.org/10.1002/2016jb013007>
- Save H (2019) GRACE follow-on (CSR-GRFO-19-01 (GRACE-FO D-103920)) (gravity recovery and climate experiment follow-on), CSR level-2 processing standards document (Rev. 1.1, June 06, 2019), (for level-2 product release 06), Center for Space Research, The University of Texas at Austin
- Scanlon BR, Zhang Z, Reedy RC, Pool DR, Save H, Long D, Chen J, Wolock DM, Conway BD, Winester D (2015) Hydrologic implications of GRACE satellite data in the Colorado River Basin. *Water Resour Res* 51:9891–9903. <https://doi.org/10.1002/2015WR018090>
- Scanlon BR, Zhang Z, Save H, Wiese DN, Landerer FW, Long D, Longuevergne L, Chen J (2016) Global evaluation of new GRACE mascons products for hydrologic applications. *Water Resour Res* 52:9412–9429. <https://doi.org/10.1002/2016WR019494>
- Scanlon BR, Zhang Z, Save H, Sun AY, Schmied HM, van Beek LPH, Wiese DN, Wada Y, Long D, Reedy RC, Longuevergne L, Döll P, Bierkens MFP (2018) Global models underestimate large decadal declining and rising water storage trends relative to GRACE satellite data. *Proc Natl Acad Sci* 115(6):E1080–E1089. <https://doi.org/10.1073/pnas.1704665115>
- Scanlon BR, Ratab A, Anyamba A, Kebede S, MacDonald AM, Shamsudduha M, Small J, Sun A, Taylor RG, Xie H (2022) Linkages between GRACE water storage, hydrologic extremes, and climate teleconnections in major African aquifers. *Environ Res Lett* 17:014046. <https://doi.org/10.1088/1748-9326/ac3bfc>
- Schmied MH, Caceres D, Eisner S, Flörke M, Herbert C, Niemann C, Peiris TA, Popat E, Portmann FT, Reinecke R, Schumacher M, Shadkam S, Telteu C-E, Trautmann T, Döll P (2021) The global water resources and use model WaterGAP v2.2d: model description and evaluation. *Geosci Model Dev* 14:1037–1079. <https://doi.org/10.5194/gmd-14-1037-2021>
- Secci D, Tanda MG, D'Oria M, Todaro V, Fagandini C (2021) Impacts of climate change on groundwater droughts by means of standardized indices and regional climate models. *J Hydro* 603(D):127154. <https://doi.org/10.1016/j.jhydrol.2021.127154>
- Shafer BA, Dezman LE (1982) Development of a surface water supply index (SWSI) to assess the severity of drought conditions in snowpack runoff areas. In: Proceedings of the Western snow conference, pp. 164–175.
- Spinoni J, Naumann G, Vogt JV, Barbosa P (2015) The biggest drought events in Europe from 1950 to 2012. *J Hydro Regional Studies* 3:509–524. <https://doi.org/10.1016/j.ejrh.2015.01.001>
- Stuhne GR, Peltier WR (2015) Reconciling the ICE-6G_C reconstruction of glacial chronology with ice sheet dynamics: the cases of Greenland and Antarctica. *J Geophys Res Earth Surface* 120(9):1841–1865. <https://doi.org/10.1002/2015JF003580>
- Sun AY, Green R, Swenson S, Rodell M (2012) Toward calibration of regional groundwater models using GRACE data. *J Hydrol* 422:1–9. <https://doi.org/10.1016/j.jhydrol.2011.10.025>
- Sun Y, Riva R, Ditmar P (2016) Optimizing estimates of annual variations and trends in geocenter motion and J2 from a combination of GRACE data and geophysical models. *J Geophys Res Solid Earth*. <https://doi.org/10.1002/2016JB013073>
- Sutton PJH (2018) Effects of climate change on sea temperature relevant to the Pacific Islands. *Sci Rev* 2018:20–30
- Tangdamrongsub N (2023) Comparative analysis of global terrestrial water storage simulations: assessing CABLE, Noah-MP, PCR-GLOBWB, and GLDAS performances during the GRACE and GRACE-FO Era. *Water* 15(13):2456. <https://doi.org/10.3390/w15132456>
- Tangdamrongsub N, Jasinski MF, Shellito PJ (2021) Development and evaluation of 0.05° terrestrial water storage estimates using community atmosphere biosphere land exchange (CABLE) land surface model and assimilation of GRACE data. *Hydro Earth Sys Sci* 25(7):4185–4208
- Tapley BD, Bettadpur S, Watkins M, Reigber C (2004) The gravity recovery and climate experiment: mission overview and early results. *Geophys Res Lett*. <https://doi.org/10.1029/2004gl019920>
- Tapley BD, Watkins MM, Flechtner F, Reigber C, Bettadpur S (2019) Contributions of GRACE to understanding climate change. *Nat Clim Chang* 9:358–369. <https://doi.org/10.1038/s41558-019-0456-2>
- Taylor I, Burke EJ, Mccoll L, Falloon P, Harris GR, McNeill D (2012) Contributions to uncertainty in projections of future drought under climate change scenarios. *Hydro Earth Syst Sci Disc* 9(11):12613–12653. <https://doi.org/10.5194/hessd-9-12613-2012>
- Tian Q, Lu J, Chen X (2022) A novel comprehensive agricultural drought index reflecting time lag of soil moisture to meteorology: a case study in the Yangtze River basin. *China Catena* 209:105804. <https://doi.org/10.1016/j.catena.2021.105804>
- Ukkola AM, De Kauwe MG, Roderick ML, Abramowitz G, Pitman AJ (2020) Robust future changes in meteorological drought in CMIP6 projections despite uncertainty in precipitation. *Geophys Res Lett* 47(11):087820. <https://doi.org/10.1029/2020gl087820>
- Ulbrich U, Brücher T, Fink AH, Leckebusch GC, Krüger A, Pinto JG (2003) The central European floods of August 2002: part 1—rainfall periods and flood development. *Weather* 58(10):371–377. <https://doi.org/10.1029/10.1256/wea.61.03A>
- Upton G, Cook I (1996) *Understanding statistics*. Oxford University Press, Oxford, p 55 (ISBN 0-19-914391-9)
- van Loon A, Laaha G (2015) Hydrological drought severity explained by climate and catchment characteristics. *J Hydro* 526:3–14. <https://doi.org/10.1016/j.jhydrol.2014.10.059>
- van Loon AF, Rangecroft S, Coxon G, Werner M, Wanders N, Baldassarre GD, Tjeldeman E, Bosman M, Gleeson T, Nauditt A, Aghakouchak A, Breña-Naranjo JA, Cenobio-Cruz O, Costa AC, Fendekova M, Jewitt G, Kingston

- DG, Loft J, Mager SM, Mallakpour I, Masih I, Maureira-Cortés H, Toth E, Oel PV, Ogtrop FV, Verbist K, Vidal J-P, Wen L, Yu M, Yuan X et al (2022) Streamflow droughts aggravated by human activities despite management. *Environ Res Lett* 17:044059. <https://doi.org/10.1088/1748-9326/ac5def>
- Vicente-Serrano SM, Beguería S, López-Moreno JI (2010) A multiscalar drought index sensitive to global warming: the standardized precipitation evapotranspiration index. *J Clim* 23:1696–1718. <https://doi.org/10.1175/2009JCLI2909.1>
- Vogel C, Koch I, Van Zyl K (2010) “A persistent truth” – reflections on drought risk management in Southern Africa. *Weather Clim Soc* 2:9–22. <https://doi.org/10.1175/2009WCAS1017.1>
- Wahr J, Molenaar M, Bryan F (1998) Time variability of the Earth's gravity field: hydrological and oceanic effects and their possible detection using GRACE. *J Geophys Res* 103:30205–30229. <https://doi.org/10.1029/98JB02844>
- Walker DW, Vergopolan N, Cavalcante L, Smith KS, Agoungbome SMD, Almagro A, Apurv T, Dahal NM, Hoffmann D, Singh V, Xiang Z (2023) Flash drought typologies and societal impacts: a worldwide review of occurrence, nomenclature, and experiences of local populations. *Weather Clim Soc* 16(1):3–28. <https://doi.org/10.1175/WCAS-D-23-0015.1>
- Wang S-Y, Chen JL, Wilson CR, Li J, Hu X (2017) Reconciling GRACE and GPS estimates of long-term load deformation in southern Greenland. *Geophys J Int* 212(2):1302–1313. <https://doi.org/10.1093/gji/ggx473>
- Wang W, Shen Y, Wang F, Li W (2021) Two severe prolonged hydrological droughts analysis over Mainland Australia using GRACE satellite data. *Remote Sens* 13(8):1432. <https://doi.org/10.3390/rs13081432>
- Wang S-Y, Li J, Chen J, Hu X-G (2022) On the improvement of mass load inversion with GNSS horizontal deformation: a synthetic study in central China. *J Geophys Res Solid Earth* 127(10):e2021JB023696. <https://doi.org/10.1029/2021JB023696>
- Watkins MM, Wiese DN, Yuan D-N, Boening C, Landerer FW (2015) Improved methods for observing Earth's time variable mass distribution with GRACE using spherical cap mascons. *J Geophys Res Solid Earth*. <https://doi.org/10.1002/2014JB011547>
- Wehner M, Seneviratne S, Zhang X, Adnan M, Badi W, Dereczynski C, Di Luca A, Ghosh S, Iskandar I, Kossin J, Lewis S, Otto F, Pinto I, Masaki S, Vicente-Serrano S, Zhou B, Hauser M, Kirchmeier-Young M, Wan H (2021) Weather and climate extreme events in a changing climate. U13B-11.
- Wessel P, Luis JF, Uieda L, Scharroo LR, Wobbe F, Smith WHF, Tian D (2019) The generic mapping tools version 6. *Geochem Geophys Geosyst* 20:5556–5564. <https://doi.org/10.1029/2019GC008515>
- Xu L, Chen N, Zhang X (2019) Global drought trends under 1.5 and 2 °C warming. *Int J Climatol* 39(4):375–2385. <https://doi.org/10.1002/joc.5958>
- Yao CH, Shum CK, Luo Z, Li Q, Lin X, Xu CH, Zhang Y, Chen J, Huang Q, Chen Y (2022) An optimized hydrological drought index integrating GNSS displacement and satellite gravimetry data. *J Hydro* 614(B):128647. <https://doi.org/10.1016/j.jhydrol.2022.128647>
- Yuan D-N (2018) GRACE (GRACE 327–744 (v 6.0) (gravity recovery and climate experiment follow-on), JPL level–2 processing standards document, for level–2 product release 06 (June 01, 2018), Jet Propulsion Laboratory, California Institute of Technology.
- Yuan D-N (2019) GRACE Follow-On (JPL D-103921) (gravity recovery and climate experiment follow-on), JPL level–2 processing standards document, for level–2 product release 06 (May 28, 2019), Jet propulsion laboratory, California Institute of Technology.
- Zeder J, Fischer EM (2020) Observed extreme precipitation trends and scaling in Central Europe. *Weather Clim Ext*. <https://doi.org/10.1016/j.wace.2020.100266>
- Zeng J, Li J, Lu Z, Wei Z, Shangguan W, Zhang S, Dai Y, Zhang S (2022) Assessment of global meteorological, hydrological and agricultural drought under future warming based on CMIP6. *Atmospheric Ocean Sci Lett* 15(1):100143. <https://doi.org/10.1016/j.aosl.2021.100143>
- Zhang Y, He B, Guo L, Liu D (2019) Differences in response of terrestrial water storage components to precipitation over 168 global River Basins. *J Hydrometeo* 20(9):1981–1999. <https://doi.org/10.1175/JHM-D-18-0253.1>
- Zhang Q, Han LY, Zeng J, Wang X, Lin JJ (2020) Climate factors during key periods affect the comprehensive crop losses due to drought in southern China. *Clim Dynam* 55:2313–2325. <https://doi.org/10.1007/s00382-020-05379-z>
- Zhao MGA, Velicogna I, Kimball JS (2017) A global gridded dataset of GRACE drought severity index for 2002–2014: comparison with PDSI and SPEI and a case study of the Australia Millennium drought. *J Hydrometeorol* 18:2117–2129. <https://doi.org/10.1175/JHM-D-16-0182.1>
- Zhong Y, Tian B, Vishwakarma BD, Feng W, Wu Y, Bai H, Zhong M (2023) Reinterpreting global GRACE trends based on century-long GRACE-REC data. *Wat Resour Res*. <https://doi.org/10.1029/2023WR035817>

Publisher's Note

Springer Nature remains neutral with regard to jurisdictional claims in published maps and institutional affiliations.